URS: A UNIFIED NEURAL ROUTING SOLVER FOR CROSS-PROBLEM ZERO-SHOT GENERALIZATION

Anonymous authors
Paper under double-blind review

ABSTRACT

Multi-task neural routing solvers have emerged as a promising paradigm for their ability to solve multiple vehicle routing problems (VRPs) using a single model. However, existing neural solvers typically rely on predefined problem constraints or require per-problem fine-tuning, which substantially limits their zero-shot generalization ability to unseen VRP variants. To address this critical bottleneck, we propose URS, a unified neural routing solver capable of zero-shot generalization across a wide range of unseen VRPs using a single model without any fine-tuning. The key component of URS is the unified data representation (UDR), which replaces problem enumeration with data unification, thereby broadening the problem coverage and reducing reliance on domain expertise. In addition, we propose a Mixed Bias Module (MBM) to efficiently learn the geometric and relational biases inherent in various problems. On top of the proposed UDR, we further develop a parameter generator that adaptively adjusts the decoder and bias weights of MBM to enhance zero-shot generalization. Moreover, we propose an LLM-driven constraint satisfaction mechanism, which translates raw problem descriptions into executable stepwise masking functions to ensure solution feasibility. Extensive experiments demonstrate that URS can consistently produce high-quality solutions for more than 100 distinct VRP variants composed of 10 different constraints without any fine-tuning, which includes more than 90 unseen variants. To the best of our knowledge, URS is the first neural solver capable of handling over 100 VRP variants with a single model.

1 INTRODUCTION

The Vehicle Routing Problem (VRP) is an essential class of combinatorial optimization problems (COPs) with extensive applications in logistics and supply chain management (Tiwari & Sharma, 2023; Sar & Ghadimi, 2023). Solving VRPs efficiently is challenging due to their NP-hard nature. While exact solvers can produce optimal solutions, they often become computationally prohibitive for real-world scenarios. In recent decades, classical heuristic solvers (Helsgaun, 2017; Vidal, 2022) have achieved impressive performance within acceptable timeframes. Nevertheless, these methods require considerable domain expertise to design specialized rules for each routing problem. Given the growing diversity of VRP variants in real-world applications, manually crafting tailored rules for every case has become impractical.

In recent years, neural combinatorial optimization (NCO) methods have attracted substantial attention for their potential to reduce reliance on handcrafted rules while maintaining competitive solution quality (Bengio et al., 2021; Li et al., 2022a). This has led to the development of many high-performing neural routing solvers that can automatically learn implicit problem-specific patterns from data under different training paradigms such as supervised learning (SL) (Drakulic et al., 2023; Luo et al., 2023; 2025b), reinforcement learning (RL) (Bello et al., 2016; Kool et al., 2019; Zhou et al., 2024a), and emerging self-improved learning (SIL) (Luo et al., 2023; 2025a; Pirnay & Grimm, 2024). Although these solvers have demonstrated impressive performance on specific problems (Kwon et al., 2020; Kim et al., 2022; Zhou et al., 2025), they typically require architectural customization and per-problem retraining to accommodate the distinct constraints and features of different VRP variants. These limitations increase the overall training cost and hinder practical deployment on new problems.

Table 1: Comparison between our URS and existing neural solvers with multi-task learning.

Neural Solver	Training Paradigm	Routing Problems (#)	Zero-shot Generalization	Remarks
MTPOMO (Liu et al., 2024a)	RL	16	✓	Constraint Combination
MVMoE (Zhou et al., 2024b)	RL	16	✓	Constraint Combination
RouteFinder (Berto et al., 2024)	RL	48	✓	Constraint Combination
CaDA (Li et al., 2025a)	RL	16	✓	Constraint Combination
MTL-KD (Zheng et al., 2025a)	RL+KD	16	✓	Constraint Combination
TSP-FT (Lin et al., 2024)	RL	3	×	Adapter-based Fine-tuning
MTL-MAB (Wang et al., 2025a)	RL	3	×	Adapter-based Fine-tuning
GOAL (Drakulic et al., 2025)	SL	9	×	Adapter-based Fine-tuning
URS (Ours)	**RL**	**107**	✓	**Unified Data Representation**

To address the challenge of cross-problem generalization, growing attention has been directed toward multi-task learning capable of handling diverse routing problems. As summarized in Table 1, existing efforts largely fall into two categories: 1) constraint combination-based multi-task learning and 2) adapter-based fine-tuning frameworks. In the first approach, VRP variants are treated as different combinations of constraint attributes, and a unified model is trained across these combinations to enable knowledge sharing for problems with seen constraints (Liu et al., 2024a; Zhou et al., 2024b; Li et al., 2025a; Berto et al., 2024; Zheng et al., 2025a). The second approach builds a shared model backbone for all problems and incorporates specific input/output adapters for each problem, thereby reducing the retraining costs (Lin et al., 2024; Drakulic et al., 2025; Wang et al., 2025a).

Despite the above advancements, existing methods still fall short in zero-shot generalization. The problem coverage of constraint combination-based approaches is inherently bounded by their manually specified constraint sets, while adapter-based approaches require fine-tuning and thus cannot perform zero-shot generalization. Moreover, both strategies fundamentally rely on the explicit enumeration of problems through a predefined set of problem tags. This practice is problematic because the constraint space of routing problems is open-ended and compositional, making any fixed tagging scheme fundamentally limited. More critically, creating and maintaining such a problem taxonomy requires considerable domain expertise, which is precisely what NCO always aims to avoid. A detailed review of related work on single-task and multi-task learning is provided in Appendix A.

In this paper, we propose a powerful **U**nified Neural **R**outing **S**olver (URS) to significantly improve the cross-problem zero-shot generalization ability for NCO methods. Unlike existing approaches, we introduce a unified data representation (UDR) that replaces problem enumeration with data unification, thereby broadening problem coverage and reducing reliance on domain expertise. In addition, we propose a Mixed Bias Module (MBM) to better learn the geometric and relational biases inherent in various problems. Based on UDR, we further develop a parameter generator that adaptively adjusts decoder and bias weights of MBM to improve zero-shot generalization. Furthermore, to handle complex and unseen routing problems, we introduce a constraint satisfaction mechanism that leverages a large language model (LLM) to translate raw problem constraint descriptions into executable node masking functions for each construction step, thereby ensuring our URS generates feasible solutions for various problems.

We evaluate URS on **more than 100** VRP variants composed of 10 different constraints, including **more than 90** unseen variants. The results demonstrate that URS not only obtains competitive performance against specialized neural solvers on seen variants but also exhibits strong zero-shot generalization capabilities on a wide range of unseen problems. To the best of our knowledge, URS is the first neural solver capable of efficiently solving over 100 distinct VRP variants using a single model without any retraining or fine-tuning.

2 Preliminaries

In this section, we first introduce the definition of VRP, then provide an overview of recent constructive neural solvers for solution generation (Kool et al., 2019; Kwon et al., 2020).

2.1 Vehicle Routing Problems

Consider a VRP instance with an optional depot indexed by 0 and n customers indexed by $\{1, 2, \ldots, n\}$, such as in the Capacitated VRP (CVRP). The instance can be represented as a graph

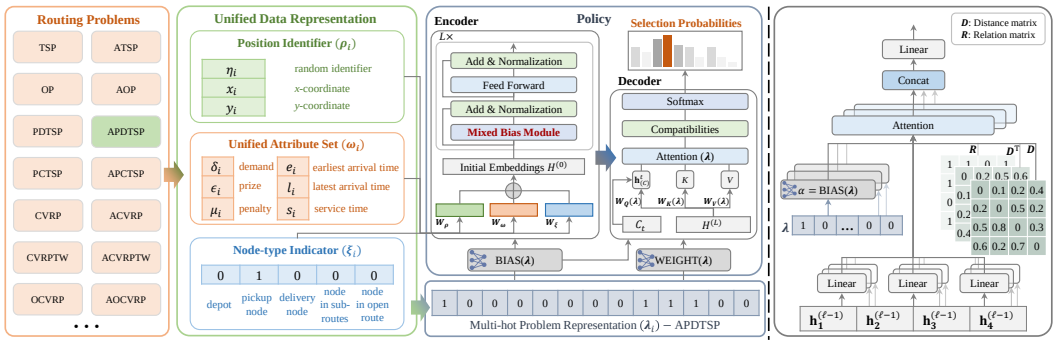

(a) The pipeline of Unified Neural Routing Solver (b) Mixed Bias Module

Figure 1: The overview of our URS with a 4-node APDTSP instance as an example. (a) The solving pipeline of URS; (b) The proposed mixed bias module that incorporates multiple geometric priors, enabling it to efficiently learn the geometric and relational biases inherent in various problems.

$\mathcal{G} = (\mathcal{V}, \mathcal{E})$, where the node set $\mathcal{V} = \{v_i\}_{i=0}^{n}$ has a total size of $|\mathcal{V}| = 1 + n$ unless the variant has no depot (e.g., the Traveling Salesman Problem), and the edge set is $\mathcal{E} = \{e(v_i, v_j) \mid v_i, v_j \in \mathcal{V}, v_i \neq v_j\}$. The travel cost between nodes is given by a distance matrix $\boldsymbol{D} = \{d_{ij} | \forall\, i, j \in 0, \ldots, n\}$. In VRP, each node $v_i \in \mathcal{V}$ includes node coordinates $\{x_i, y_i\}$ when available and problem-specific attributes (e.g., demands in CVRP). A feasible solution of a VRP calls for the determination of a set of routes, each performed by a single vehicle that starts and ends at its own depot or starting node, all the operational constraints are satisfied, denoted as $\boldsymbol{\pi} = (\pi_1, \pi_2, \ldots, \pi_m)$ (Toth & Vigo, 2002) (i.e., a finite sequence), which is a permutation of m nodes. Let Ω denote the feasible sequence set that satisfies the constraints, given an objective function $f(\boldsymbol{\pi}|\mathcal{G})$, we aim to search for a sequence $\boldsymbol{\pi}^*$ with the maximum objective, i.e., $\boldsymbol{\pi}^* = \arg\max_{\boldsymbol{\pi} \in \Omega} f(\pi|\mathcal{G})$. In most routing problems, the objective can be represented as the negative value of the total distance of a feasible sequence $\boldsymbol{\pi}$.

In this paper, we consider over 100 VRP variants which may simultaneously have one or more constraints from the following categories: (1) Capacity (C); (2) Open Route (O); (3) Backhaul (B); (4) Backhaul and Priority (BP); (5) Duration Limit (L); (6) Time Windows (TW); (7) Multi-Depot (MD); (8) Prize Collecting (PC); (9) Asymmetric (A); (10) Pickup and Delivery (PD). Detailed definitions of these constraints are provided in Appendix B.

2.2 Constructive Neural Routing Solver

Most constructive NCO methods employ an encoder-decoder architecture for solution construction (Luo et al., 2023; Kwon et al., 2020). Let learnable model parameters be denoted as $\boldsymbol{\theta} = \{\boldsymbol{\theta}_{enc}, \boldsymbol{\theta}_{dec}\}$. Without loss of generality, we present the prevailing construction pipeline using AM (Kool et al., 2019). Given an instance $\mathcal{G}$, raw node features are first mapped by a linear projection to initial embeddings $H^{(0)} = \{\mathbf{h}_i^{(0)}\}_{i=0}^{n}$. They are then processed by an encoder $\boldsymbol{\theta}_{enc}$ with L attention layers to produce refined node embeddings $H^{(L)} = \{\mathbf{h}_i^{(L)}\}_{i=0}^{n}$. At each decoding step t, the decoder $\boldsymbol{\theta}_{dec}$ sequentially selects a node to append to the current partial solution $\pi_{1:t-1} = (\pi_1, \pi_2, ..., \pi_{t-1})$, where $\pi_1, \pi_{t-1} \in \mathcal{V}$ are the **first** and **last** visited node, respectively. This sequential process continues until a complete solution is formed. To guarantee the feasibility of generated solutions, a masking function $\mathcal{M}_t$ sets the selection probabilities of the following nodes to $-\infty$ during the construction process: nodes that (1) are visited or (2) violate problem-specific constraints (e.g., capacity).

3 The Proposed Model: Unified Neural Routing Solver

In this section, we propose a powerful **U**nified Neural **R**outing **S**olver (URS), which can significantly improve cross-problem zero-shot generalization for NCO methods. The framework is illustrated in Figure 1, and its key components are elaborated below.

3.1 UNIFIED DATA REPRESENTATION

Existing multi-task neural solvers (Liu et al., 2024a; Zhou et al., 2024b; Drakulic et al., 2025; Wang et al., 2025a) fundamentally rely on the explicit problem enumeration through a predefined set of problem tags, which is challenging because the constraint space of routing problems is open-ended and compositional, making any fixed tagging scheme fundamentally limited. More critically, creating and maintaining such a problem taxonomy requires considerable domain expertise, which is precisely what NCO always aims to avoid.

From a data perspective, despite the substantial diversity in constraints among routing problems, their instances share a common instance representation, e.g., all input instances under the current constraint combinations (Liu et al., 2024a; Zhou et al., 2024b) can be formulated as instances of either CVRP or CVRPTW. Leveraging this commonality, we propose a Unified Data Representation (UDR) to replace problem enumeration with data unification, thereby broadening problem coverage and reducing reliance on domain expertise. For an instance $\mathcal{G}$, we define the unified representation $\boldsymbol{U} = \{\mathbf{u}_i\}_{i=0}^{n}$, each $\mathbf{u}_i = \{\boldsymbol{\rho}_i,\ \boldsymbol{\omega}_i,\ \boldsymbol{\xi}_i\}$, where $\boldsymbol{\rho}_i,\ \boldsymbol{\omega}_i,\ \boldsymbol{\xi}_i$ are a position identifier, unified attribute set, and node-type indicator, respectively.

Position Identifier ($\boldsymbol{\rho}_i$) We define a unified positional identifier for each node as $\boldsymbol{\rho}_i = \{\eta_i, x_i, y_i\} \in [0,1]^3$. The $\eta_i \sim \text{Uniform}(0,1) \in \mathbb{R}^1$ is an additional sampled scalar, which is used to address asymmetric problems, following Drakulic et al. (2023). For symmetric cases, we simply set $\eta_i = 0$.

Unified Attribute Set ($\boldsymbol{\omega}_i$) We define the unified attribute set as $\boldsymbol{\omega}_i = \{\delta_i, \epsilon_i, \mu_i,\ e_i,\ l_i,\ s_i\}$, where they correspond to demand, prize, penalty, earliest arrival time, latest arrival time, and service time, respectively. The unification empowers the model to learn the relative importance of individual attributes in a shared embedding space. Furthermore, it supports effortless extension or ablation of attributes through simple zero-filling, which eliminates the need for changes to the model architecture.

Node-type Indicator ($\boldsymbol{\xi}_i$) We provide an additional 5-dimensional binary vector $\boldsymbol{\xi}_i \in \{0,1\}^5$ for each node, encoding: depot, pickup node, delivery node, node in sub-routes, node in open route. The nodes in sub-routes and open routes mean the solution π can have sub-routes or be an open route. We introduce explicit structural roles via $\boldsymbol{\xi}_i$ that help the model generalize over diverse routing problems. Further ablation analysis concerning $\boldsymbol{\xi}_i$ can be found in Appendix K.1.

Relation Matrix ($\boldsymbol{R}$) To facilitate the handling of Pickup and Delivery (PD) problems, we introduce an optional relation matrix $\boldsymbol{R}$, which is applied exclusively to variants involving PD constraints. We define $\boldsymbol{R} = \{r_{ij} | \ \forall\ i, j \in 0, \ldots, n\}$, where $r_{ij} = 0$ if a predefined relation exists (e.g., pickup–delivery pairing in PDPs) and 1 otherwise. This ensures that smaller values are preferred, aligning with the distance metric where a smaller value corresponds to a larger selection bias.

Multi-hot Problem Representation ($\boldsymbol{\lambda}_i$) Through the UDR, each problem instance activates only a specific subset of the unified feature space. Thus, for any instance $\mathcal{G}_i$ drawn from different problems, a corresponding multi-hot problem representation $\boldsymbol{\lambda}i$ is obtained by indicating active (non-zero) feature slots with a value of 1. This representation captures only the presence of features, in contrast to their raw values, and it subsequently provides conditional guidance to the position bias weight (see Equation (6)) and the adaptive decoder parameters $\boldsymbol{\theta}_{dec}(\boldsymbol{\lambda})$ (see Equation (8) and Equation (9)), thereby helping the model in distinguishing problem variants and refining its node selection process.

Instead of relying on a predefined problem taxonomy with a discrete set of problem tags, our proposed UDR decouples instance representation from constraint definitions and operates in a unified space characterized by both continuous and discrete features. It allows a single neural solver to address a much larger, open-ended space of VRP variants, as new problems can be seamlessly incorporated into this unified representation. Problem-specific constraints are delegated to the model-agnostic masking function $\mathcal{M}_t$. For example, for all capacity-constrained problems, only the remaining load is explicitly provided as input, while diverse additional constraints (e.g., time windows, duration limit, and backhaul) are enforced implicitly by masking infeasible candidate nodes during solution construction, rather than being fully enumerated in the decoder's input. This process is further automated by an LLM-driven constraint satisfaction mechanism that generates problem-specific mask generators, which convert constraint handling from manual engineering to automated programming

(see Section 4 for more details). Together, our proposed UDR enables a single model to handle various explored and even unexplored VRP variants while significantly reducing reliance on domain expertise. Detailed descriptions of $\boldsymbol{U}$ and $\boldsymbol{\lambda}$ are provided in Appendix C and Appendix D, respectively.

3.2 Model Architecture

As shown in Figure 1, we adopt AM (Kool et al., 2019) as our basic model. While UDR provides cross-problem consistency, different problems have diverse geometric priors. To efficiently learn the geometric and relational biases inherent in various problems and obtain better generalization performance, we propose two key enhancements: (1) Mixed Bias Modules (MBM) that integrate diverse geometric priors, and (2) adaptive parameter generators conditioned on the UDR. Their implementations are detailed below.

Embedding Layer Given an instance $\mathcal{G}$, for each $\mathbf{u}_i = \{\boldsymbol{\rho}_i,\ \boldsymbol{\omega}_i,\ \boldsymbol{\xi}_i\}$, we project each component into d-dimensional embeddings through three separate linear transformations:

$$\mathbf{h}_i^{(0)} = \boldsymbol{\rho}_i W_{\boldsymbol{\rho}} + \boldsymbol{\omega}_i W_{\boldsymbol{\omega}} + \boldsymbol{\xi}_i W_{\boldsymbol{\xi}}, \tag{1}$$

where $W_{\boldsymbol{\rho}} \in \mathbb{R}^{3\times d},\ W_{\boldsymbol{\omega}} \in \mathbb{R}^{6\times d},\ W_{\boldsymbol{\xi}} \in \mathbb{R}^{5\times d}$ are learnable matrices. Then we obtain a set of initial embeddings $H^{(0)} = \{\mathbf{h}_i^{(0)}\}_{i=0}^{n}$ for all nodes in instance $\mathcal{G}$.

Encoder The encoder $\boldsymbol{\theta}_{enc}$ with L stacked attention layers transforms $H^{(0)}$ into advanced node embeddings $H^{(L)} = \{\mathbf{h}_i^{(L)}\}_{i=0}^{n}$. The detailed process is provided in Appendix E.1. Unlike prior work, we replace the plain attention (Vaswani et al., 2017) with the proposed mixed bias module (MBM) that incorporates three structural bias matrices via three separate attention calculations: (1) an outgoing distance matrix $\boldsymbol{D}$; (2) an incoming distance matrix $\boldsymbol{D}^{\mathbf{T}}$; and (3) optional relation matrix $\boldsymbol{R}$, For the ℓ-th layer, the MBM output $\hat{\mathbf{h}}_i^{(\ell)}$ can be expressed as:

$$\bar{\mathbf{h}}_i^{(0)} = \mathrm{Attention}(\mathbf{h}_i^{(\ell-1)}, H^{(\ell-1)}, f\left(\alpha, N, \boldsymbol{D}_i\right)), \tag{2}$$

$$\bar{\mathbf{h}}_i^{(1)} = \mathrm{Attention}(\mathbf{h}_i^{(\ell-1)}, H^{(\ell-1)}, f\left(\alpha, N, \boldsymbol{D}_i^{\mathrm{T}}\right)), \tag{3}$$

$$\bar{\mathbf{h}}_i^{(2)} = \begin{cases} \mathrm{Attention}(\mathbf{h}_i^{(\ell-1)}, H^{(\ell-1)}, f\left(\alpha, \boldsymbol{R}_i\right)) & \text{if } \boldsymbol{R} \neq \emptyset \\ \mathbf{0} & \text{otherwise,} \end{cases}, \tag{4}$$

$$\hat{\mathbf{h}}_i^{(\ell)} = \left[\hat{\mathbf{h}}_i^{(0)}, \hat{\mathbf{h}}_i^{(1)}, \hat{\mathbf{h}}_i^{(2)}\right] W^O, \tag{5}$$

where $[\cdot,\cdot]$ denotes the horizontal concatenation operator, $W^O \in \mathbb{R}^{(3\times d)\times d}$ is a learnable matrices. For $\mathrm{Attention}(\cdot)$, we adopt the Adaptation Attention Free Module (AAFM) (Zhou et al., 2024a), which boosts the perception of diverse geometric patterns through an adaptation function $f(\alpha, N, d_{ij})$ with bias weight α (see Appendix F for implementation details). We generate α via a lightweight bias network $\mathrm{BIAS}(\boldsymbol{\lambda})$ whose input is the instance's multi-hot representation $\boldsymbol{\lambda}$:

$$\mathrm{BIAS}(\boldsymbol{\lambda}) = \max\left(1,\ \left(\boldsymbol{\lambda} W_1 + \mathbf{b}_1\right) W_2 + \mathbf{b}_2\right), \tag{6}$$

where $W_1 \in \mathbb{R}^{|\boldsymbol{\lambda}|\times d},\ W_2 \in \mathbb{R}^{d\times 1},\ \mathbf{b}_1 \in \mathbb{R}^{d},\ \mathbf{b}_2 \in \mathbb{R}^{1}$ are learnable parameters. We set the minimum value of the generated bias to 1, resulting in faster model convergence. Due to the relation r_{ij} is scale-independent, we remove scale N in adaptation function for $\boldsymbol{R}$, and if $\boldsymbol{R}$ is absent, we substitute a zero vector for $\bar{\mathbf{h}}_i^{(2)}$.

As shown in Figure 1(b), the Mixed Bias Module (MBM) is introduced to address the limitations of standard attention mechanisms in capturing geometric and relational biases inherent in diverse routing problems. For example, effectively representing asymmetric distances in AVRPs or pairing relationships in PDPs remains challenging, which hinders the achievement of high-quality solutions across a wide range of problems. While prior work, such as MatNet (Kwon et al., 2021), has proposed addressing this limitation by incorporating distance biases from different directions in separate parallel layers, this design leads to high model complexity and is only applicable to ATSP. In contrast, our MBM innovatively integrates multiple geometric priors (e.g., D, D^T, relation matrix R) within a single shared attention layer. This integrated design enhances flexibility while reducing architectural redundancy.

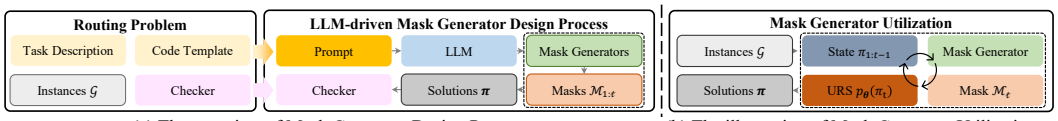

(a) The overview of Mask Generator Design Process (b) The illustration of Mask Generator Utilization

Figure 3: The overview of LLM-driven Constraint Satisfaction Mechanism. (a) The generating pipeline of LLM-driven Constraint Satisfaction Mechanism for a general routing problem; (b) The illustration of mask generator utilization, handling the complex constraint.

Decoder In URS, all parameters of $\boldsymbol{\theta}_{dec}(\boldsymbol{\lambda})$ are generated based on the multi-hot problem representation $\boldsymbol{\lambda}$. Following Kwon et al. (2020), given the first and last visited node embeddings $\mathbf{h}_{\pi_1}^{(L)}$ and $\mathbf{h}_{\pi_{t-1}}^{(L)}$, and an optional constraint state $C_t \in \mathbb{R}^1$ (e.g., remaining load), the context embedding $\mathbf{h}_{(C)}^t$ can be expressed as:

$$\mathbf{h}_{(C)}^t = \left[\mathbf{h}_{\pi_1}^{(L)},\ \mathbf{h}_{\pi_{t-1}}^{(L)},\ C_t\right] W_Q(\boldsymbol{\lambda}), \tag{7}$$

where $[\cdot,\cdot]$ is the horizontal concatenation operator, $W_Q(\boldsymbol{\lambda}) \in \mathbb{R}^{(2d+1)\times d}$ is a linear projection matrix conditioned on $\boldsymbol{\lambda}$. Missing C_t is zero-padded (see Appendix E.3 for detailed settings). The new context embedding $\hat{\mathbf{h}}_{(C)}^t$ is obtained via $\mathrm{Attention}(\cdot)$ (Zhou et al., 2024a) on $\mathbf{h}_{(C)}^t$ and $H^{(L)}$:

$$\hat{\mathbf{h}}_{(C)}^t = \mathrm{Attention}(\mathbf{h}_{(C)}^t, H^{(L)}W_K(\boldsymbol{\lambda}), H^{(L)}W_V(\boldsymbol{\lambda}), \mathcal{M}_t, f(\alpha, N, d_{t,i})), \tag{8}$$

where $W_K(\boldsymbol{\lambda}) \in \mathbb{R}^{d\times d}$, $W_V(\boldsymbol{\lambda}) \in \mathbb{R}^{d\times d}$ are linear projection matrices conditioned on $\boldsymbol{\lambda}$. Finally, we compute the selection probability for each feasible node $p_{\boldsymbol{\theta}}(\pi_t = i \mid \mathcal{G}, \pi_{1:t-1})$ based on the improved compatibility with adaptation bias (Zhou et al., 2024a):

$$p_{\boldsymbol{\theta}}(\pi_t = i \mid \mathcal{G}, \pi_{1:t-1}) = \mathrm{softmax}(\zeta \cdot \tanh(\frac{\hat{\mathbf{h}}_{(C)}^t (\mathbf{h}_i^{(L)})^{\mathrm{T}}}{\sqrt{d}} + f(\alpha, N, d_{t,i})) + \mathcal{M}_t) \tag{9}$$

where ζ is the clipping parameter. Inspired by Lin et al. (2022), we use a simple MLP hypernetwork $\mathrm{WEIGHT}(\boldsymbol{\lambda})$ to generate $\{W_Q(\boldsymbol{\lambda}),\ W_K(\boldsymbol{\lambda}),\ W_V(\boldsymbol{\lambda})\}$ (see Appendix E.2 for implementation details). For α in Equation (8) and Equation (9), we generate them via $\mathrm{BIAS}(\boldsymbol{\lambda})$ in Equation (6).

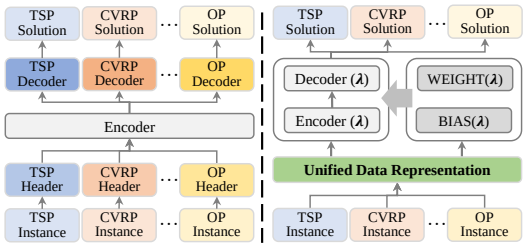

(a) Adapter-based Fine-tuning (b) URS (Ours)

Figure 2: Comparison between our URS and existing adapter-based fine-tuning frameworks.

As shown in Figure 2, using a model with a single static set of parameters to solve over 100 diverse VRP variants is challenging and prone to underfitting. To mitigate this, we introduce a problem-adaptive mechanism consisting of two components: (1) $\mathrm{BIAS}(\lambda)$ dynamically adjusts how the model integrates different geometric priors in the attention mechanism based on the problem representation λ; and (2) $\mathrm{WEIGHT}(\lambda)$ generates adaptive decoder parameters for each problem. Unlike existing adapter-based fine-tuning methods (Lin et al., 2024; Drakulic et al., 2025; Wang et al., 2025a), URS adaptively generates the decoder parameters for each problem, thereby enabling the generation of high-quality solutions without requiring retraining or fine-tuning.

4 LLM-DRIVEN CONSTRAINT SATISFACTION MECHANISM

While the proposed UDR enables URS to handle a wide range of routing problems, ensuring solution feasibility across diverse and potentially unseen constraints remains a major challenge. Traditional NCO approaches rely on manually designed masks $\mathcal{M}_t$ for each specific VRP variant Kool et al. (2019); Kwon et al. (2020); Luo et al. (2023), which becomes impractical when solving over 100 distinct variants as targeted by URS. To address this bottleneck, we propose an LLM-driven constraint satisfaction mechanism that automatically produces problem-specific **mask generators**. This mechanism transforms constraint handling from a manual engineering task into an automated program design task, thereby effectively supporting URS's excellent zero-shot generalization capabilities.

As illustrated in Figure 3 (a), our constraint satisfaction mechanism operates through a systematic generate-and-validate pipeline. Notably, the generation of mask generators within this pipeline is performed offline: the process begins by prompting an LLM (we adopt GPT-3.5-turbo for this work, though this model selection is not mandatory—alternative models are equally competent, with only differences in computational efficiency) with both a clear and concise problem-specific natural language constraint description that explicitly articulates the task's core constraints and objectives and a standardized Python code template with well-defined input/output interfaces. The LLM then designs a set of candidate mask generators that implement the constraint logic. Each candidate is validated on a set of problem instances using a problem-specific checker to verify its reliability in producing feasible solutions. Invalid candidates are discarded, and the generation process iterates until a reliable mask generator is obtained.

Specifically, during validation, the candidate mask generator guides the stepwise solution construction. As illustrated in Figure 3 (b), at each step t, the mask generator takes the current state of the partial solution $\pi_{1:t-1}$ as input, which contains various information such as visited nodes, remaining load, etc. It then produces a binary mask $\mathcal{M}_t$ that identifies all permissible nodes. This mask is directly integrated into the URS's selection probability computation in Equation 9 to ensure feasibility.

To efficiently steer this generate-and-test process, we formulate it as an optimization problem that maximizes the solution validity rate. The well-developed LLM-based automated algorithm design frameworks, such as EoH (Liu et al., 2024b), can be effectively applied to tackle this optimization problem. The optimization process terminates immediately once a reliable mask generator is found, which significantly reduces computational overhead compared to exhaustive search approaches. Furthermore, generated mask generators can be cached and reused for different instances sharing the same problem variant, thereby amortizing the generation cost. For more details about our LLM-driven constraint satisfaction mechanism, please see Appendix G.

5 Experiments

In this section, we comprehensively evaluate URS against classical and learning-based solvers across more than one hundred distinct VRP variants. For URS, we focus on: (1) performance on seen problems and (2) zero-shot generalization under unseen ones. To ensure comparability with prior neural routing studies, we adopt the 100-node setting as our primary evaluation scenario for URS. All experiments are conducted on a single NVIDIA GeForce RTX 4090 GPU (24GB memory).

5.1 Experimental Setup

Problem Setting We train URS on 11 mixed VRP variants to ensure that each feature in UDR has been seen at least once, i.e., $\mathcal{P} = \{P_i\}_{i=1}^{11}$ (see Appendix J.1 for more discussion about problem selection). Specifically, training problems and related data generations are as follows: (1) ATSP (Kwon et al., 2021);(2) TSP (Kool et al., 2019); (3) CVRP (Kool et al., 2019); (4) ACVRP (Kwon et al., 2021; Kool et al., 2019); (5) Orienteering Problem (OP) (Kool et al., 2019); (6) PCTSP (Kool et al., 2019); (7) PDTSP (Li et al., 2021); (8) CVRPTW (Zhou et al., 2024b); (9) OCVRP (Zhou et al., 2024b); (10) CVRPB (Zhou et al., 2024b), and (11) OCVRPTW (Zhou et al., 2024b). To evaluate the zero-shot generalization of URS, we construct 96 unseen variants to further highlight the broad applicability of URS. And each test dataset consists of 1000 instances. The oracle solver for each problem can be found in Appendix D.

Model & Training Setting We use an embedding dimension d of 128 and a feed-forward layer dimension of 512. We set the number of attention layers in the encoder to 12. The clipping parameter $\zeta = 50$ in Equation (9) for better training convergence (Jin et al., 2023). For training, URS is trained by the REINFORCE (Williams, 1992) algorithm, and the data is generated on the fly (see Appendix E.4 for more details). We train URS for 500 epochs with 2,000 batches per epoch, and the batch size is 128. At each training step, we randomly select one problem P_i from the problem set $\mathcal{P}$. We employ the AdamW optimizer (Loshchilov & Hutter, 2017) with an initial learning rate of 10^{-4}, which is decayed by a factor of 0.1 at the 451st epoch. Weight decay is set to 10^{-6}. More details about the model training are provided in Appendix H.

Table 2: Performance on 1K test instances of 11 seen VRPs.

Method	ATSP		TSP		OP		PCTSP		PDTSP		–	
	Gap	Time	Gap	Time	Gap	Time	Gap	Time	Gap	Time		
Oracle Solver	0.00%	2m	0.00%	6m	0.00%	1.5m	0.00%	1.2h	0.00%	9.8m	–	
Sym-NCO	–		0.14%	5s	0.68%	15s	0.14%	16s	–		–	
BQ	1.27%	1m	0.35%	7s	0.63%	7s	–		–		–	
LEHD	–		0.59%	2s	–		–		–		–	
POMO	–		0.13%	5s	–		–		–		–	
ICAM	3.05%	1m	0.15%	4s	–		–		–		–	
MatNet	0.95%	6.5m	–		–		–		–		–	
Heter-AM	–		–		–		–		6.61%	5m	–	
GOAL-MTL	1.77%	1m	–		1.20%	38s	–		–		–	
URS-STL	**0.62%**	1.1m	**0.08%**	6s	**0.11%**	4s	**-0.09%**	5s	**3.22%**	4s	–	
URS	2.26%	1.1m	0.57%	6s	0.45%	4s	1.06%	5s	4.98%	4s	–	

Method	ACVRP		CVRP		CVRPTW		CVRPB		OCVRP		OCVRPTW	
	Gap	Time	Gap	Time	Gap	Time	Gap	Time	Gap	Time	Gap	Time
Oracle Solver	0.00%	6.6m	0.00%	9.1m	0.00%	19.6m	0.00%	20.8m	0.00%	5.3m	0.00%	20.8m
Sym-NCO	–		1.46%	6s	–		–		–		–	
BQ	–		3.24%	8s	–		–		–		–	
LEHD	–		3.68%	2s	–		–		–		–	
POMO	–		**1.25%**	6s	–		–		–		–	
ICAM	–		2.04%	4s	–		–		–		–	
MVMoE	–		1.65%	12s	4.90%	15s	1.28%	11s	3.14%	13s	3.85%	15s
MTPOMO	–		1.85%	6s	5.31%	8s	1.67%	5s	3.46%	6s	4.41%	7s
ReLD-MTL	–		1.42%	8s	4.56%	10s	**0.90%**	6s	2.32%	7s	**3.10%**	9s
GOAL-MTL	–		4.22%	48s	4.66%	42s	–		–		–	
URS-STL	**2.01%**	1.4m	1.63%	6s	**4.50%**	8s	1.59%	6s	**2.25%**	6s	3.22%	8s
URS	3.06%	1.4m	1.81%	6s	6.13%	8s	1.46%	6s	3.24%	6s	5.07%	8s

Baseline We compare URS with the following methods: (1)**Classical Solvers:**[1] PyVRP (Wouda et al., 2024), LKH3 (Helsgaun, 2017), and OR-Tools (Perron & Furnon, 2023); (2)**Neural Solvers:** (i) *specialized solvers that support multiple VRP variants*: Sym-NCO (Kim et al., 2022), BQ (Drakulic et al., 2023), LEHD (Luo et al., 2023), ICAM (Zhou et al., 2024a) and POMO (Kwon et al., 2020); (ii) *general neural solvers capable of handling multiple variants*[2]: MTPOMO (Liu et al., 2024a), MVMoE (Zhou et al., 2024b), ReLD-MTL (Huang et al., 2025), GOAL-MTL (Drakulic et al., 2025); (iii) *Solvers for less-explored variants*: MatNet (Kwon et al., 2021), Heter-AM (Li et al., 2021).

Metrics and Inference We report the average objective value (Obj.), optimality gap (Gap), and total inference time (Time) for each method. The optimality gap quantifies the discrepancy between the solutions generated by the corresponding methods and the near-optimal solutions, which are obtained using classical solvers. For most NCO baseline methods, we execute the source code provided by the authors using default settings. We compare the performance of URS to the relevant baselines for each problem as well as its single-task version (i.e., URS-STL). For more details about URS-STL, please see Appendix H.2. For symmetric instances, we report the best result with $\times 8$ instance augmentation, following Kwon et al. (2020). For asymmetric instances, we report the best result with $\times 128$ instance augmentation, following Kwon et al. (2021). Furthermore, we also verify the performance of URS under different evaluation scenarios (e.g., Sym-NCO (Kim et al., 2022)), please see Appendix J.2 for more results.

5.2 Performance Evaluation

Performance on Seen VRPs The experimental results on trained VRPs with scale 100 are reported in Table 2. We observe that among all comparable neural solvers, URS-STL achieves the best performance on 8 out of the 11 routing problems, complemented by remarkably fast inference,

[1]We run LKH3 (Helsgaun, 2017) with 10000 trials and 1 run (Kool et al., 2019). For PyVRP and OR-Tools, we run them on a single CPU core with time limits of 20s (Li et al., 2025a).

[2]Given the differences in problem variants and visible task training among the baseline models, we only compare methods with the same training setup. Thus, RF (Berto et al., 2024) and CaDA (Li et al., 2025a) are not included in our experiments to ensure a fair comparison.

Table 3: Zero-shot generalization on 1K test instances of 30 unseen VRPs. Due to page limit, complete experimental results (including all 96 unseen variants) are deferred to Appendix I.

Method	CVRPBP		OCVRPBP		CVRPBPL		OCVRPBPTW		CVRPBPLTW	
	Gap	Time	Gap	Time	Gap	Time	Gap	Time	Gap	Time
Oracle Solver	0.00%	6.6m	0.00%	6.6m	0.00%	6.6m	0.00%	6.6m	0.00%	6.6m
MVMoE	13.95%	14s	17.36%	14s	13.38%	14s	2.29%	15s	10.46%	16s
MTPOMO	13.71%	7s	16.94%	8s	13.44%	8s	3.26%	9s	11.35%	10s
ReLD-MTL	13.57%	9s	14.83%	9s	12.96%	10s	2.27%	11s	10.80%	12s
URS	**12.95%**	7s	**14.30%**	7s	**12.65%**	8s	**-3.47%**	8s	**9.74%**	10s

Method	MDCVRP		MDCVRPL		MDOCVRPB		MDOCVRPBPTW		MDOCVRPBPLTW	
	Gap	Time	Gap	Time	Gap	Time	Gap	Time	Gap	Time
Oracle Solver	0.00%	6.6m	0.00%	6.6m	0.00%	6.6m	0.00%	6.6m	0.00%	6.6m
MVMoE	31.90%	31s	33.42%	44s	28.21%	26s	46.18%	40s	45.23%	40s
MTPOMO	23.75%	27s	24.32%	25s	25.06%	20s	34.19%	29s	33.37%	31s
ReLD-MTL	17.37%	36s	18.48%	28s	18.50%	21s	34.08%	33s	33.83%	36s
URS	**9.65%**	22s	**15.32%**	26s	**15.17%**	18s	**11.17%**	25s	**10.96%**	28s

Method	ACVRPB		ACVRPL		ACVRPTW		AOPDCVRP		ACVRPBL	
	Gap	Time	Gap	Time	Gap	Time	Gap	Time	Gap	Time
Oracle Solver	0.00%	6.6m	0.00%	6.6m	0.00%	6.6m	0.00%	6.6m	0.00%	6.6m
URS	**7.10%**	2.1m	**-2.24%**	1.9m	**11.28%**	2.5m	**11.13%**	1.2m	**6.18%**	2.4m

Method	AOCVRPBPTW		ACVRPBPLTW		ACVRPBPTW		AOCVRPBPLTW		ACVRPBTW	
	Gap	Time	Gap	Time	Gap	Time	Gap	Time	Gap	Time
Oracle Solver	0.00%	6.6m	0.00%	6.6m	0.00%	6.6m	0.00%	6.6m	0.00%	6.6m
URS	**3.28%**	2.5m	**-0.58%**	2.8m	**0.12%**	2.5m	**2.54%**	2.7m	**9.95%**	2.2m

Method	AMDCVRPL		AMDCVRPBPLTW		AMDOCVRPBPLTW		PDCVRP		OPDCVRP	
	Gap	Time	Gap	Time	Gap	Time	Gap	Time	Gap	Time
Oracle Solver	0.00%	6.6m	0.00%	6.6m	0.00%	6.6m	0.00%	6.6m	0.00%	6.6m
URS	**7.15%**	6.1m	**4.45%**	8.3m	**8.63%**	7.5m	**-1.47%**	4.3s	**4.93%**	4.3s

Method	AMDOCVRPBPTW		AMDCVRPBPTW		AMDCVRP		APDTSP		APDCVRP	
	Gap	Time	Gap	Time	Gap	Time	Gap	Time	Gap	Time
Oracle Solver	0.00%	6.6m	0.00%	6.6m	0.00%	6.6m	0.00%	6.6m	0.00%	6.6m
URS	**9.61%**	6.9m	**4.63%**	7.6m	**3.56%**	5.3m	**6.21%**	1m	**7.03%**	1.2m

highlighting the strength of the URS architecture when fully specialized. Meanwhile, mixing all problems into the training of URS incurs only a minor performance drop, yet still delivers competitive performance across all problems, demonstrating that potential connections among different problems are effectively captured by URS.

Generalization to Unseen VRPs We evaluate our URS model on zero-shot generalization across 96 unseen VRP variants, including 44 well-studied VRP variants from the NCO community and 52 newly introduced variants that have not been explored before. The detailed results are presented in Table 3 and Appendix I. On widely-studied constraints (i.e., C, O, L, TW, MD, B, BP), URS continues to deliver high-quality solutions. Notably, URS merely selects the next node from a given feasible candidates without any additional domain knowledge, making its performance especially meaningful. Benefiting from our UDR, URS can directly address previously unexplored variants while maintaining solution quality, which compounds asymmetry and PD relations. Without any fine-tuning, URS still constructs high-quality solutions for more than 90 VRP variants that are not seen in training, highlighting its strong zero-shot generalization ability.

Results on Benchmark Dataset We further evaluate the generalization ability of URS on benchmark instances from CVRPLIB Set-X (Uchoa et al., 2017) with scale $\in [500, 1000]$ and large-scale CVRPLib XXL (Arnold et al., 2019) benchmark dataset with scale $\in [3000, 7000]$, and we compare URS against several representative single-task and multi-task models. As demonstrated in Appendix J.3, URS maintains its position as the best overall performance across instances of varying scales in Set-X dataset. For CVRPLib XXL benchmark. The results clearly demonstrate that URS can significantly outperform existing multi-task neural routing solvers, especially on large-scale instances. Notably, URS also greatly surpasses many representative specialized models (e.g., LEHD, BQ, and ELG). These results further underscore the practical applicability of URS in real-world scenarios.

Scalability to Larger-scale Realistic Problems Due to the limited benchmark datasets currently available for VRP variants, we have conducted further experiments on large-scale synthetic problem instances to validate the large-scale cross-problem generalization ability of URS. We generate a new large-scale (1K-5K nodes) synthetic dataset for a diverse set of problems (CVRPTW, CVRPB, and OCVRPTW). According to the results in Appendix J.4, our proposed URS consistently achieves the best solution quality, complemented by remarkably fast inference times, across various problem instances among all comparable neural solvers. The advantages of URS over existing multi-task neural solvers are significant. Remarkably, URS already outperforms the strong HGS-PyVRP with a carefully manual design on large-scale CVRPB instances. These extensive results demonstrate URS's strong scalability and generalization ability to large-scale and realistic problems.

6 Ablation Study

In this section, we conduct an ablation study across 11 seen VRP variants to validate the effect of key components of URS, mainly including: (1) without node-type indicator $\boldsymbol{\xi}$ of UDR; (2) without problem state C_t; (3) effects of different priors in MBM ; (4) effects of alternative decoder architectures. As detailed in Table 4. URS maintains its competitive performance without C_t. And its effectiveness is further improved by the inclusion of a node-type indicator $\boldsymbol{\xi}$. For MBM, the results reveal that three priors $\{\boldsymbol{D}, \boldsymbol{D}^{\mathbf{T}}, \boldsymbol{R}\}$ are complementary, and their combined use allows MBM to effectively learn the geometric and relational biases inherent in various problems, resulting in superior overall performance. Furthermore, replacing the decoder with POMO or ReLD confirms the strong cross-problem robustness of URS, while the integration of the decoder in ICAM (Zhou et al., 2024a) leads to a further improvement. More detailed results and analyses can be found in Appendix K.

Table 4: Effects of different components of URS.

Method	Avg.gap
w/o $\boldsymbol{\xi}$	3.78%
w/o C_t	2.97%
$\{\boldsymbol{D}\}$	6.33%
$\{\boldsymbol{D}, \boldsymbol{D}^{\mathbf{T}}\}$	4.07%
$\{\boldsymbol{D}, \boldsymbol{R}\}$	7.34%
POMO-Dec.	3.39%
ReLD-Dec.	3.87%
URS	**2.74%**

To empirically evaluate the necessity of our proposed components (MBM, WEIGHT(λ), and BIAS(λ)), we have conducted tests on the 11 seen problems as well as 11 additional unseen CVRP variants widely investigated in current multi-task research (e.g., MVMoE (Zhou et al., 2024b)). As shown in Appendix K.4, the full URS model achieves the lowest average gap and provides the best solution on the majority of tasks (19/22). This demonstrates that the synergy of these components is essential for robust cross-problem generalization.

7 Conclusion, Limitation, and Future Work

In this work, we propose a novel RL-based Unified Routing Solver (URS) for cross-problem zero-shot generalization. The core of URS is a Unified Data Representation (UDR), which broadens problem coverage by substituting problem enumeration with data unification. Its generalization capability is further enhanced by a Mixed Bias Module (MBM) and an adaptive parameter generator. Moreover, an LLM-based constraint satisfaction mechanism guarantees solution feasibility and reduces dependency on domain expertise. Extensive experiments demonstrate that URS can produce high-quality solutions for more than 100 distinct VRP variants composed of 10 different constraints without any fine-tuning, more than 90 of which are unseen during training.

Limitation and Future Work While URS achieves impressive results on a wide range of VRP variants, its current training scheme does not accommodate their inherent differences in complexity and randomly selects one problem at each training step. In addition, the UDR can produce highly similar representations for problems that share similar attributes but involve significantly different dynamic constraints (e.g., CVRP vs. CVRPL). This ambiguity may challenge the parameter generator and impair zero-shot performance on such variants. In the future, we aim to explore more effective training schemes to further improve training efficiency and design more robust unified data representation.

REFERENCES

Florian Arnold, Michel Gendreau, and Kenneth Sörensen. Efficiently solving very large-scale routing problems. *Computers & operations research*, 107:32–42, 2019.

Irwan Bello, Hieu Pham, Quoc V Le, Mohammad Norouzi, and Samy Bengio. Neural combinatorial optimization with reinforcement learning. *arXiv preprint arXiv:1611.09940*, 2016.

Yoshua Bengio, Andrea Lodi, and Antoine Prouvost. Machine learning for combinatorial optimization: a methodological tour d'horizon. *European Journal of Operational Research*, 290(2):405–421, 2021.

Federico Berto, Chuanbo Hua, Nayeli Gast Zepeda, André Hottung, Niels Wouda, Leon Lan, Junyoung Park, Kevin Tierney, and Jinkyoo Park. Routefinder: Towards foundation models for vehicle routing problems. *arXiv preprint arXiv:2406.15007*, 2024.

Yuanyao Chen, Rongsheng Chen, Fu Luo, and Zhenkun Wang. Improving generalization of neural combinatorial optimization for vehicle routing problems via test-time projection learning. *arXiv preprint arXiv:2506.02392*, 2025.

Pham Vu Tuan Dat, Long Doan, and Huynh Thi Thanh Binh. Hsevo: Elevating automatic heuristic design with diversity-driven harmony search and genetic algorithm using llms. In *Proceedings of the AAAI Conference on Artificial Intelligence*, volume 39, pp. 26931–26938, 2025.

Darko Drakulic, Sofia Michel, Florian Mai, Arnaud Sors, and Jean-Marc Andreoli. Bq-nco: Bisimulation quotienting for efficient neural combinatorial optimization. In *Thirty-seventh Conference on Neural Information Processing Systems*, 2023.

Darko Drakulic, Sofia Michel, and Jean-Marc Andreoli. Goal: A generalist combinatorial optimization agent learner. In *The Thirteenth International Conference on Learning Representations*, 2025.

Han Fang, Zhihao Song, Paul Weng, and Yutong Ban. Invit: A generalizable routing problem solver with invariant nested view transformer. In *International Conference on Machine Learning*, 2024.

Zhang-Hua Fu, Kai-Bin Qiu, and Hongyuan Zha. Generalize a small pre-trained model to arbitrarily large tsp instances. In *Proceedings of the AAAI Conference on Artificial Intelligence*, volume 35, pp. 7474–7482, 2021.

Chengrui Gao, Haopu Shang, Ke Xue, Dong Li, and Chao Qian. Towards generalizable neural solvers for vehicle routing problems via ensemble with transferrable local policy. In *International Joint Conference on Artificial Intelligence*, 2024.

David Ha, Andrew Dai, and Quoc V Le. Hypernetworks. *arXiv preprint arXiv:1609.09106*, 2016.

Kaiming He, Xiangyu Zhang, Shaoqing Ren, and Jian Sun. Deep residual learning for image recognition. In *Proceedings of the IEEE Conference on Computer Vision and Pattern Recognition*, pp. 770–778, 2016.

Keld Helsgaun. An extension of the lin-kernighan-helsgaun tsp solver for constrained traveling salesman and vehicle routing problems. *Roskilde: Roskilde University*, 12, 2017.

Qingchun Hou, Jingwei Yang, Yiqiang Su, Xiaoqing Wang, and Yuming Deng. Generalize learned heuristics to solve large-scale vehicle routing problems in real-time. In *The Eleventh International Conference on Learning Representations*, 2022.

Ziwei Huang, Jianan Zhou, Zhiguang Cao, and Yixin Xu. Rethinking light decoder-based solvers for vehicle routing problems. *International Conference on Learning Representations*, 2025.

Yan Jin, Yuandong Ding, Xuanhao Pan, Kun He, Li Zhao, Tao Qin, Lei Song, and Jiang Bian. Pointerformer: Deep reinforced multi-pointer transformer for the traveling salesman problem. In *The Thirty-Seventh AAAI Conference on Artificial Intelligence*, 2023.

Minsu Kim, Junyoung Park, and Jinkyoo Park. Sym-nco: Leveraging symmetricity for neural combinatorial optimization. *Advances in Neural Information Processing Systems*, 35:1936–1949, 2022.

Detian Kong, Yining Ma, Zhiguang Cao, Tianshu Yu, and Jianhua Xiao. Efficient neural collaborative search for pickup and delivery problems. *IEEE Transactions on Pattern Analysis and Machine Intelligence*, 2024.

Wouter Kool, Herke van Hoof, and Max Welling. Attention, learn to solve routing problems! In *International Conference on Learning Representations*, 2019.

Yeong-Dae Kwon, Jinho Choo, Byoungjip Kim, Iljoo Yoon, Youngjune Gwon, and Seungjai Min. Pomo: Policy optimization with multiple optima for reinforcement learning. *Advances in Neural Information Processing Systems*, 33:21188–21198, 2020.

Yeong-Dae Kwon, Jinho Choo, Iljoo Yoon, Minah Park, Duwon Park, and Youngjune Gwon. Matrix encoding networks for neural combinatorial optimization. *Advances in Neural Information Processing Systems*, 34:5138–5149, 2021.

Bingjie Li, Guohua Wu, Yongming He, Mingfeng Fan, and Witold Pedrycz. An overview and experimental study of learning-based optimization algorithms for the vehicle routing problem. *IEEE/CAA Journal of Automatica Sinica*, 9(7):1115–1138, 2022a.

Han Li, Fei Liu, Zhi Zheng, Yu Zhang, and Zhenkun Wang. Cada: Cross-problem routing solver with constraint-aware dual-attention. In *Proceedings of the 42nd International Conference on Machine Learning*, 2025a.

Jingwen Li, Liang Xin, Zhiguang Cao, Andrew Lim, Wen Song, and Jie Zhang. Heterogeneous attentions for solving pickup and delivery problem via deep reinforcement learning. *IEEE Transactions on Intelligent Transportation Systems*, 23(3):2306–2315, 2021.

Jingwen Li, Yining Ma, Ruize Gao, Zhiguang Cao, Andrew Lim, Wen Song, and Jie Zhang. Deep reinforcement learning for solving the heterogeneous capacitated vehicle routing problem. *IEEE Transactions on Cybernetics*, 52(12):13572–13585, 2022b.

Ke Li, Fei Liu, Zhenkun Wang, and Qingfu Zhang. Destroy and repair using hyper-graphs for routing. In *Proceedings of the AAAI Conference on Artificial Intelligence*, volume 39, pp. 18341–18349, 2025b.

Yang Li, Jinpei Guo, Runzhong Wang, and Junchi Yan. T2t: From distribution learning in training to gradient search in testing for combinatorial optimization. In *Thirty-seventh Conference on Neural Information Processing Systems*, 2023.

Xi Lin, Zhiyuan Yang, and Qingfu Zhang. Pareto set learning for neural multi-objective combinatorial optimization. In *10th International Conference on Learning Representations*, 2022.

Zhuoyi Lin, Yaoxin Wu, Bangjian Zhou, Zhiguang Cao, Wen Song, Yingqian Zhang, and Senthilnath Jayavelu. Cross-problem learning for solving vehicle routing problems. In *Proceedings of the Thirty-Third International Joint Conference on Artificial Intelligence*, pp. 6958–6966, 2024.

Fei Liu, Xi Lin, Zhenkun Wang, Qingfu Zhang, Tong Xialiang, and Mingxuan Yuan. Multi-task learning for routing problem with cross-problem zero-shot generalization. In *Proceedings of the 30th ACM SIGKDD Conference on Knowledge Discovery and Data Mining*, pp. 1898–1908, 2024a.

Fei Liu, Tong Xialiang, Mingxuan Yuan, Xi Lin, Fu Luo, Zhenkun Wang, Zhichao Lu, and Qingfu Zhang. Evolution of heuristics: Towards efficient automatic algorithm design using large language model. In *International Conference on Machine Learning*, pp. 32201–32223. PMLR, 2024b.

Ilya Loshchilov and Frank Hutter. Decoupled weight decay regularization. *arXiv preprint arXiv:1711.05101*, 2017.

Fu Luo, Xi Lin, Fei Liu, Qingfu Zhang, and Zhenkun Wang. Neural combinatorial optimization with heavy decoder: Toward large scale generalization. In *Thirty-seventh Conference on Neural Information Processing Systems*, 2023.

Fu Luo, Xi Lin, Yaoxin Wu, Zhenkun Wang, Tong Xialiang, Mingxuan Yuan, and Qingfu Zhang. Boosting neural combinatorial optimization for large-scale vehicle routing problems. In *The Thirteenth International Conference on Learning Representations*, 2025a.

Fu Luo, Xi Lin, Mengyuan Zhong, Fei Liu, Zhenkun Wang, Jianyong Sun, and Qingfu Zhang. Learning to insert for constructive neural vehicle routing solver. *arXiv preprint arXiv:2505.13904*, 2025b.

Fu Luo, Yaoxin Wu, Zhi Zheng, and Zhenkun Wang. Rethinking neural combinatorial optimization for vehicle routing problems with different constraint tightness degrees. *arXiv preprint arXiv:2505.24627*, 2025c.

Mohammadreza Nazari, Afshin Oroojlooy, Lawrence Snyder, and Martin Takác. Reinforcement learning for solving the vehicle routing problem. *Advances in Neural Information Processing Systems*, 31, 2018.

Laurent Perron and Vincent Furnon. Or-tools, 2023. URL `https://developers.google.com/optimization/`.

Jonathan Pirnay and Dominik G Grimm. Self-improvement for neural combinatorial optimization: Sample without replacement, but improvement. *Transactions on Machine Learning Research*, 2024.

Ruizhong Qiu, Zhiqing Sun, and Yiming Yang. Dimes: A differentiable meta solver for combinatorial optimization problems. *Advances in Neural Information Processing Systems*, 35:25531–25546, 2022.

Kubra Sar and Pezhman Ghadimi. A systematic literature review of the vehicle routing problem in reverse logistics operations. *Computers & Industrial Engineering*, 177:109011, 2023.

Rui Sun, Zhi Zheng, and Zhenkun Wang. Learning encodings for constructive neural combinatorial optimization needs to regret. In *Proceedings of the AAAI Conference on Artificial Intelligence*, volume 38, pp. 20803–20811, 2024.

Zhiqing Sun and Yiming Yang. Difusco: Graph-based diffusion solvers for combinatorial optimization. *Advances in Neural Information Processing Systems*, 36:3706–3731, 2023.

Krishna Veer Tiwari and Satyendra Kumar Sharma. An optimization model for vehicle routing problem in last-mile delivery. *Expert Systems with Applications*, 222:119789, 2023.

Paolo Toth and Daniele Vigo. *The vehicle routing problem*. SIAM, 2002.

Eduardo Uchoa, Diego Pecin, Artur Pessoa, Marcus Poggi, Thibaut Vidal, and Anand Subramanian. New benchmark instances for the capacitated vehicle routing problem. *European Journal of Operational Research*, 257(3):845–858, 2017.

Dmitry Ulyanov, Andrea Vedaldi, and Victor Lempitsky. Instance normalization: The missing ingredient for fast stylization. *arXiv preprint arXiv:1607.08022*, 2016.

Ashish Vaswani, Noam Shazeer, Niki Parmar, Jakob Uszkoreit, Llion Jones, Aidan N Gomez, Łukasz Kaiser, and Illia Polosukhin. Attention is all you need. *Advances in Neural Information Processing Systems*, 30, 2017.

Thibaut Vidal. Hybrid genetic search for the cvrp: Open-source implementation and swap* neighborhood. *Computers & Operations Research*, 140:105643, 2022.

Oriol Vinyals, Meire Fortunato, and Navdeep Jaitly. Pointer networks. *Advances in Neural Information Processing Systems*, 28, 2015.

Chenguang Wang, Zhang-Hua Fu, Pinyan Lu, and Tianshu Yu. Efficient training of multi-task neural solver for combinatorial optimization. *Transactions on Machine Learning Research*, 2025a.

Yang Wang, Ya-Hui Jia, Wei-Neng Chen, and Yi Mei. Distance-aware attention reshaping for enhancing generalization of neural solvers. *IEEE Transactions on Neural Networks and Learning Systems*, 2025b.

Ronald J Williams. Simple statistical gradient-following algorithms for connectionist reinforcement learning. *Machine Learning*, 8:229–256, 1992.

Niels A Wouda, Leon Lan, and Wouter Kool. Pyvrp: A high-performance vrp solver package. *INFORMS Journal on Computing*, 36(4):943–955, 2024.

Yubin Xiao, Di Wang, Boyang Li, Huanhuan Chen, Wei Pang, Xuan Wu, Hao Li, Dong Xu, Yanchun Liang, and You Zhou. Reinforcement learning-based nonautoregressive solver for traveling salesman problems. *IEEE Transactions on Neural Networks and Learning Systems*, 2024a.

Yubin Xiao, Di Wang, Boyang Li, Mingzhao Wang, Xuan Wu, Changliang Zhou, and You Zhou. Distilling autoregressive models to obtain high-performance non-autoregressive solvers for vehicle routing problems with faster inference speed. In *Proceedings of the AAAI Conference on Artificial Intelligence*, volume 38, pp. 20274–20283, 2024b.

Liang Xin, Wen Song, Zhiguang Cao, and Jie Zhang. Step-wise deep learning models for solving routing problems. *IEEE Transactions on Industrial Informatics*, 17(7):4861–4871, 2020.

Chengrun Yang, Xuezhi Wang, Yifeng Lu, Hanxiao Liu, Quoc V Le, Denny Zhou, and Xinyun Chen. Large language models as optimizers. In *The Twelfth International Conference on Learning Representations*, 2023.

Haoran Ye, Jiarui Wang, Zhiguang Cao, Helan Liang, and Yong Li. Deepaco: Neural-enhanced ant systems for combinatorial optimization. *Advances in neural information processing systems*, 36: 43706–43728, 2023.

Haoran Ye, Jiarui Wang, Zhiguang Cao, Federico Berto, Chuanbo Hua, Haeyeon Kim, Jinkyoo Park, and Guojie Song. Reevo: Large language models as hyper-heuristics with reflective evolution. *Advances in neural information processing systems*, 37:43571–43608, 2024a.

Haoran Ye, Jiarui Wang, Helan Liang, Zhiguang Cao, Yong Li, and Fanzhang Li. Glop: Learning global partition and local construction for solving large-scale routing problems in real-time. In *Proceedings of the AAAI Conference on Artificial Intelligence*, volume 38, pp. 20284–20292, 2024b.

Yuepeng Zheng, Fu Luo, Zhenkun Wang, Yaoxin Wu, and Yu Zhou. Mtl-kd: Multi-task learning via knowledge distillation for generalizable neural vehicle routing solver. *arXiv preprint arXiv:2506.02935*, 2025a.

Zhi Zheng, Shunyu Yao, Zhenkun Wang, Xialiang Tong, Mingxuan Yuan, and Ke Tang. Dpn: Decoupling partition and navigation for neural solvers of min-max vehicle routing problems. In *Proceedings of the 41st International Conference on Machine Learning*, pp. 61559–61592, 2024a.

Zhi Zheng, Changliang Zhou, Tong Xialiang, Mingxuan Yuan, and Zhenkun Wang. Udc: A unified neural divide-and-conquer framework for large-scale combinatorial optimization problems. In *Thirty-eighth Conference on Neural Information Processing Systems*, 2024b.

Zhi Zheng, Zhuoliang Xie, Zhenkun Wang, and Bryan Hooi. Monte carlo tree search for comprehensive exploration in llm-based automatic heuristic design. *arXiv preprint arXiv:2501.08603*, 2025b.

Changliang Zhou, Xi Lin, Zhenkun Wang, Xialiang Tong, Mingxuan Yuan, and Qingfu Zhang. Instance-conditioned adaptation for large-scale generalization of neural routing solver. *arXiv preprint arXiv:2405.01906*, 2024a.

Changliang Zhou, Xi Lin, Zhenkun Wang, and Qingfu Zhang. Learning to reduce search space for generalizable neural routing solver. *arXiv preprint arXiv:2503.03137*, 2025.

Jianan Zhou, Zhiguang Cao, Yaoxin Wu, Wen Song, Yining Ma, Jie Zhang, and Chi Xu. Mvmoe: multi-task vehicle routing solver with mixture-of-experts. In *Proceedings of the 41st International Conference on Machine Learning*, pp. 61804–61824, 2024b.

A Related Work

A.1 Neural Routing Solvers with Single-Task Learning

The NCO methods have emerged as a promising paradigm for tackling various routing problems, achieving impressive empirical performance. Early seminal work based on Pointer Networks ignited interest in learning end-to-end construction policies for TSP and CVRP (Vinyals et al., 2015; Bello et al., 2016; Nazari et al., 2018). Subsequently, the Transformer-style heavy-encoder and light-decoder auto-regressive architecture has become the dominant paradigm (Kool et al., 2019), while POMO (Kwon et al., 2020) exploits permutation symmetry to enhance exploration diversity. Many advancements within this paradigm have pushed promising results on small instances (e.g., 100-node TSPs) (Xin et al., 2020; Kim et al., 2022; Xiao et al., 2024a;b; Sun et al., 2024). However, models trained on a fixed instance scale often degrade sharply when evaluated out of scale. To mitigate the poor generalization performance, recent studies introduce auxiliary local policies (Gao et al., 2024), adaptive perception across instance scales (Zhou et al., 2024a), or different search space reduction methods (Fang et al., 2024; Zhou et al., 2025; Chen et al., 2025). In parallel, "heavy decoder" designs that dynamically recompute embeddings at each construction step (Drakulic et al., 2023; Luo et al., 2023) demonstrate strong generalization on large-scale instances. To improve the performance on large-scale routing instances, complementary directions are reducing solving difficulty via problem decomposition (Zheng et al., 2024b; Ye et al., 2024b; Li et al., 2025b) or adopting non-autoregressive generation augmented with additional searches (e.g., Monte Carlo tree search (MCTS) and 2-opt) (Fu et al., 2021; Sun & Yang, 2023; Qiu et al., 2022; Li et al., 2023; Ye et al., 2023). Moreover, heterogeneous vehicle routing (Li et al., 2022b), asymmetric distance settings (Kwon et al., 2021), multiple VRPs (Zheng et al., 2024a), and pickup–delivery problems (Li et al., 2021; Kong et al., 2024) have each motivated tailored neural designs, which have yielded competitive results. Despite these advancements, they still train a specialized model per problem type, limiting cross-problem transfer. We instead focus on a unified neural routing solver that aims to generalize across multiple routing problems without retraining from scratch for each specification.

A.2 Neural Routing Solvers with Multi-Task Learning

To address the challenge of cross-problem generalization, growing attention has shifted to multi-task learning capable of adapting to diverse routing problems. Existing efforts can broadly fall into two categories: (1) constraint combination-based multi-task learning and (2) adapter-based fine-tuning frameworks. The former line (e.g., MTPOMO (Liu et al., 2024a)) treats VRP variants as combinations of a predefined set of attributes and trains a shared backbone, achieving promising results on up to 16 VRP variants. Follow-up work extends this paradigm by introducing mixture-of-experts (MoE) modules (Zhou et al., 2024b), heavy decoder designs plus knowledge distillation (Zheng et al., 2025a), and constraint-aware dual-attention (Li et al., 2025a) or updated Transformer structure (Berto et al., 2024) to improve model performance. While this enables knowledge sharing across problems, its coverage is inherently bounded by the hand-specified attribute set. The second family trains a shared backbone and performs adaptation to each variant via lightweight adapters. For instance, Lin et al. (2024) pretrain a TSP backbone and adapt to new variants through adapter-based fine-tuning. Drakulic et al. (2025) integrate edge features and adopt supervised multi-task pretraining for obtaining a powerful backbone before fine-tuning on novel tasks. Wang et al. (2025a) propose a multi-armed bandit strategy to realize more efficient multi-task training. Although these reduce retraining cost, they fail to achieve zero-shot generalization. In contrast, we focus on a constructive neural routing solver supported with zero-shot capability: once trained, it can directly generate high-quality solutions for previously unseen problems without any fine-tuning.

A.3 LLM-based Algorithm Generation in VRPs

Employing LLMs to solve VRPs is a new research direction. As an early attempt, Yang et al. (2023) utilizes the LLM as a direct optimizer, prompting an LLM to directly generate solutions for TSP instances. A more predominant stream leverages LLMs as automated algorithm designers to generate algorithms for solving VRPs. These methods often integrate LLMs with a search procedure. EoH (Liu et al., 2024b) combined an LLM with Evolutionary Computation to design heuristic components for a Guided Local Search (GLS) framework. ReEvo (Ye et al., 2024a) incorporated a reflection mechanism to refine heuristics for iterative solution construction. HSEvo (Dat et al.,

2025) additionally introduced a diversity mechanism for designing heuristics solving TSP and OP. And AHD-MCTS (Zheng et al., 2025b) employed Monte Carlo Tree Search (MCTS) to guide the design of heuristics for solving TSP and CVRP. Despite their promise, these methods share common limitations rooted in their reliance on the LLM's implicit, pre-trained knowledge as the core design logic. The process of discovering effective algorithms demands extensive search procedures and is computationally expensive. Furthermore, the heuristics generated by the LLM are susceptible to overfitting to the specific instances used during the design phase, limiting their generalization capabilities. In contrast, our URS overcomes these challenges by establishing a clear division of labor: the LLM is tasked with satisfying complex constraints, while our URS model is responsible for ensuring solution quality. This approach significantly reduces the reasoning burden on the LLM, mitigating the risk of overfitting and enabling URS to effectively solve a more extensive range of VRPs.

B SETUPS OF VRP VARIANTS

In this paper, we consider over 100 VRP variants which may simultaneously have one or more constraints from the following categories: (1) Capacity (C); (2) Open Route (O); (3) Backhaul (B); (4) Backhaul and Priority (BP); (5) Duration Limit (L); (6) Time Windows (TW); (7) Multi-Depot (MD); (8) Prize Collecting (PC); (9) Asymmetric (A); (10) Pickup and Delivery (PD). The node coordinates are randomly sampled from the unit square when available (in symmetric geometric cases, i.e., $d_{ij} = d_{ji}$), following AM (Kool et al., 2019). Below, we provide a comprehensive description of the data generation process for each constraint.

Capacity (C) The selection of the vehicle capacity $\mathcal{C}$ is critical, as prior work (Luo et al., 2025c) demonstrates its significant impact on the solution structure. For PDVRP variants (e.g., PDCVRP, OPDCVRP, APDCVRP, and AOPDCVRP), an excessively large $\mathcal{C}$ causes the solution to approximate that of a PDTSP instance. Conversely, an overly restrictive $\mathcal{C}$ promotes a simplistic, repetitive Pickup-Delivery sequence. To ensure structurally sound solutions, we set $\mathcal{C}$=20 for PDCVRP variants. For all other VRP variants, we adopt the convention from AM (Kool et al., 2019), setting $\mathcal{C}$=50.

Open Route (O) The open route setting implies that vehicles are not required to return to the depot after completing their service tours. This does not alter the data generation, and it specifically affects the final cost evaluation by excluding the travel distance from the last customer back to the depot.

Backhaul (B) The standard CVRP involves vehicles delivering goods from a depot to a set of customers with positive demands. The introduction of backhauls extends this formulation to the CVRP with Backhauls (CVRPB), where vehicles must also load goods from backhaul customers and return them to the depot, in addition to serving the standard linehaul (delivery) customers. Following the experimental setup of MTPOMO (Liu et al., 2024a), we generate customer demands by sampling from a discrete uniform distribution over the integers $\{1, \ldots, 9\}$. Subsequently, 20% of these nodes are randomly designated as backhaul customers, and their corresponding demand values are negative, while the remainder are classified as linehaul customers. Notably, no precedence constraints are imposed between the servicing of linehaul and backhaul customers.To ensure the feasibility of the solutions constructed by our neural solver, we adhere to the MVMoE (Zhou et al., 2024b) framework's policy that the first customer visited must be a linehaul node.

Backhaul and Priority (BP) This constraint imposes a strict precedence requirement on the standard CVRPB, dictating that all linehaul customers must be serviced prior to any backhaul customers. Consequently, once a vehicle serves a backhaul customer, it is prohibited from visiting any subsequent linehaul nodes within the same route. If the first customer served is a backhaul node, the vehicle's load is initialized to zero. This ensures the neural solver can construct a feasible solution.

Duration Limit (L) Following MTPOMO (Liu et al., 2024a), we impose a duration limit (i.e., the maximum length of each vehicle route) of 3 in symmetric cases. Since the node coordinates are randomly sampled from the unit square, the maximum possible distance between any two nodes is $\sqrt{2}$. The setting is sufficient to ensure a vehicle can deliver goods to at least one customer and return to the depot, thus guaranteeing the feasibility of the solution. For the setting of asymmetric cases, we provide details in the description of the following asymmetric instances.

Time Windows (TW) Consistent with the MVMoE (Zhou et al., 2024b), we set time windows of the depot to $[e_0, l_0]$=[0,3] and its service time to 0. The service time s_i for each customer node is set to 0.2. For the time windows for each customer node, we generate them following the methodology outlined in MVMoE (Zhou et al., 2024b).

Multi-Depot (MD) The generation of coordinates for the multiple depots aligns with that of other nodes, with the number of depots set to 3 (Berto et al., 2024). A vehicle is required to return to the same depot it departed from. To guarantee that each starting node is considered in this multi-depot variant, we set the number of trajectories for an instance to be the product of the number of depots and the number of customer nodes, maximizing the exploration of high-quality solutions.

Prize Collecting (PC) Under the Prize Collecting condition, each node (excluding the depot) is assigned both a prize and a penalty. A prize is collected for each visited node, while a penalty is incurred for each unvisited node. The objective is to minimize the total travel distance plus the sum of penalties for all unvisited nodes. A key constraint is that a minimum amount of total prize must be collected before the vehicle is permitted to return to the depot and terminate its route. Consistent with the AM (Kool et al., 2019) framework, the prizes and penalties are generated as follows: $prize \sim \text{Uniform}\left(0, \frac{4}{n}\right)$, and $penalty \sim \text{Uniform}\left(0, 3 \cdot \frac{k_n}{n}\right)$, where $n = 100$ and $k_n = 4$ in our experiments.

Asymmetric (A) We adopt the data generation method from MatNet (Kwon et al., 2021) to create an asymmetric distance matrix. Due to the small pairwise distances in the generated distance matrix, the parameters for duration limit and time windows set for symmetric cases are not applicable to the asymmetric problems. To ensure the constraints remain valid, we adjust the duration limit and depot end time to 0.6 and 1.0, respectively.

Pickup and Delivery (PD) For PDP variants, we adhere to the methodology in Li et al. (2021). For a problem of size N, node 0 is set to the depot, nodes 1 to $N/2$ are designated as pickup nodes, while nodes from $N/2 + 1$ to N are designated as delivery nodes. For each pickup node v_i, its corresponding delivery node is $v_{i+N/2}$. A strict precedence constraint is imposed in PDP cases, requiring each vehicle to visit a pickup node before its corresponding delivery node. For PDCVRP variants, the demand for each delivery node is randomly sampled from a discrete uniform distribution over $\{1, 2, \ldots, 9\}$. The demand for each pickup node is then set to the negative of its corresponding delivery node's demand. To ensure the feasibility of the constraints, the vehicle capacity is set to 20.

C UNIFIED DATA REPRESENTATION

In this section, we provide a detailed description of our UDR $\boldsymbol{U} = \{\mathbf{u}_i\}_{i=0}^{n}$ (see Table 5). Each node $\mathbf{u}_i$ consists of three components, i.e., $\mathbf{u}_i = \{\boldsymbol{\rho}_i,\ \boldsymbol{\omega}_i,\ \boldsymbol{\xi}_i\}$. where $\boldsymbol{\rho}_i,\ \boldsymbol{\omega}_i,\ \boldsymbol{\xi}_i$ are a position identifier, unified attribute set, and node-type indicator, respectively. To distinguish linehaul/delivery from backhaul/pickup nodes, we assign negative demand values to backhaul/pickup nodes (positive for linehaul/delivery), making demand the only signed component, following (Liu et al., 2024a; Zhou et al., 2024b).

Table 5: Detailed description of each component in UDR.

Attribute Name	Symbol	Range	Description	Examples
Random Identifier	η	$[0, 1]$	Random scalar for asymmetric problems.	ATSP
Node Coordinates	$\{x, y\}$	$[0, 1]^2$	2D coordinates of the node.	TSP, CVRP
Demand	δ	$[-1, 1]$	Node demand ($+$ for delivery, $-$ for pickup).	CVRP, PDCVRP
Prize	ϵ	$[0, 1]$	Prize collected for each node.	OP, PCTSP
Penalty	μ	$[0, 1]$	Penalty incurred for each node.	PCTSP
Earliest Arrival Time	e	$[0, 1]$	Earliest permissible arrival time.	CVRPTW
Latest Arrival Time	l	$[0, 1]$	Latest permissible arrival time (deadline).	CVRPTW
Service Time	s	$[0, 1]$	Time required for service at the node.	CVRPTW
Depot	$-$	$\{0, 1\}$	Indicates if the node is a depot.	CVRP
Pickup Node	$-$	$\{0, 1\}$	Indicates if the node is a pickup location.	PDTSP
Delivery Node	$-$	$\{0, 1\}$	Indicates if the node is a delivery location.	CVRP, PDTSP
Node in Sub-routes	$-$	$\{0, 1\}$	The solution π can have sub-routes.	CVRP
Node in Open Route	$-$	$\{0, 1\}$	Vehicles need not return to the depot.	OCVRP

D MULTI-HOT PROBLEM REPRESENTATION

Leveraging the UDR, each problem instance activates only a subset of the unified feature space. Thus, for any instance $\mathcal{G}_i$ from different problems, we simply mark active (non-zero) feature slots with 1 to obtain a corresponding multi-hot problem representation $\boldsymbol{\lambda}_i$. Different from raw feature values, it encodes presence only and provides conditional signals to the following position bias weight (see Equation (6)) and adaptive decoder (see Equation (8) and Equation (9)), helping the model distinguish variants and refine node selection. Here, we provide detailed representations for each problem in our experiments, and each problem is a 13-dimensional multi-hot vector.

As shown in Table 6, we train URS on eleven classic and varied routing problems to ensure that each feature in the UDR has been seen at least once, i.e., $\mathcal{P} = \{P_i\}_{i=1}^{11}$. Then, we evaluate generalization on unseen problems on different combinations of ten constraint attributes (see Appendix B), and the detailed representations of each unseen problem can be found in Table 7 (documented VRP variants) and Table 8 (undocumented VRP variants).

Table 6: The representations for seen routing problems in our experiments. The total number of problems is 11. In training, each feature in the UDR has been seen at least once. Here, RI represents the random identifier, and EAT, LAT, and ST indicate the earliest arrival time, the latest arrival time, and the service time, respectively.

Problem	Oracle	RI	Coord.	Demand	Prize	Penalty	EAT	LAT	ST	Depot	Pickup	Delivery	Sub-routes	Open Route
ATSP	LKH-3	✓												
TSP	LKH-3		✓											
OP	Compass		✓		✓					✓				
PCTSP	ILS		✓		✓	✓				✓				
PDTSP	LKH-3		✓							✓	✓	✓		
ACVRP	OR-Tools	✓		✓						✓		✓	✓	
CVRP	PyVRP		✓	✓						✓		✓	✓	
CVRPTW	PyVRP		✓	✓			✓	✓	✓	✓		✓	✓	
CVRPB	OR-Tools		✓	✓						✓	✓	✓	✓	
OCVRP	LKH-3		✓	✓						✓		✓	✓	✓
OCVRPTW	OR-Tools		✓	✓			✓	✓	✓	✓		✓	✓	✓

Table 7: The problem representations of 44 VRP variants that have been extensively explored in current literature (Liu et al., 2024a; Berto et al., 2024). Here, RI represents the random identifier, and EAT, LAT, and ST indicate the earliest arrival time, the latest arrival time, and the service time, respectively.

Problem	Oracle	RI	Coord.	Demand	Prize	Penalty	EAT	LAT	ST	Depot	Pickup	Delivery	Sub-routes	Open Route
CVRPL	LKH-3		✓	✓						✓		✓	✓	
OCVRPB	OR-Tools		✓	✓						✓	✓	✓	✓	✓
CVRPBL	OR-Tools		✓	✓						✓	✓	✓	✓	
CVRPLTW	OR-Tools		✓	✓			✓	✓	✓	✓		✓	✓	
OCVRPBTW	OR-Tools		✓	✓			✓	✓	✓	✓	✓	✓	✓	✓
CVRPBLTW	OR-Tools		✓	✓			✓	✓	✓	✓	✓	✓	✓	
OCVRPL	OR-Tools		✓	✓						✓		✓	✓	✓
CVRPBTW	OR-Tools		✓	✓			✓	✓	✓	✓	✓	✓	✓	
OCVRPBL	OR-Tools		✓	✓						✓	✓	✓	✓	✓
OCVRPLTW	OR-Tools		✓	✓			✓	✓	✓	✓		✓	✓	✓
OCVRPBLTW	OR-Tools		✓	✓			✓	✓	✓	✓	✓	✓	✓	✓
CVRPBP	OR-Tools		✓	✓						✓	✓	✓	✓	
OCVRPBP	OR-Tools		✓	✓						✓	✓	✓	✓	✓
CVRPBPL	OR-Tools		✓	✓						✓	✓	✓	✓	
OCVRPBPTW	OR-Tools		✓	✓			✓	✓	✓	✓	✓	✓	✓	✓
CVRPBLTW	OR-Tools		✓	✓			✓	✓	✓	✓	✓	✓	✓	
CVRPBPTW	OR-Tools		✓	✓			✓	✓	✓	✓	✓	✓	✓	
OCVRPBPL	OR-Tools		✓	✓						✓	✓	✓	✓	✓
OCVRPBLTW	OR-Tools		✓	✓			✓	✓	✓	✓	✓	✓	✓	✓
MDCVRP	PyVRP		✓	✓						✓		✓	✓	
MDCVRPTW	PyVRP		✓	✓			✓	✓	✓	✓		✓	✓	
MDOCVRP	PyVRP		✓	✓						✓		✓	✓	✓
MDCVRPL	PyVRP		✓	✓						✓		✓	✓	
MDCVRPB	PyVRP		✓	✓						✓	✓	✓	✓	
MDOCVRPTW	PyVRP		✓	✓			✓	✓	✓	✓		✓	✓	✓
MDOCVRPB	PyVRP		✓	✓						✓	✓	✓	✓	✓
MDCVRPBL	PyVRP		✓	✓						✓	✓	✓	✓	
MDCVRPLTW	PyVRP		✓	✓			✓	✓	✓	✓		✓	✓	
MDOCVRPBTW	PyVRP		✓	✓			✓	✓	✓	✓	✓	✓	✓	✓
MDCVRPBLTW	PyVRP		✓	✓			✓	✓	✓	✓	✓	✓	✓	
MDOCVRPL	PyVRP		✓	✓						✓		✓	✓	✓
MDCVRPBTW	PyVRP		✓	✓			✓	✓	✓	✓	✓	✓	✓	
MDOCVRPBL	PyVRP		✓	✓						✓	✓	✓	✓	✓
MDOCVRPLTW	PyVRP		✓	✓			✓	✓	✓	✓		✓	✓	✓
MDOCVRPBLTW	PyVRP		✓	✓			✓	✓	✓	✓	✓	✓	✓	✓
MDCVRPBP	PyVRP		✓	✓						✓	✓	✓	✓	
MDOCVRPBP	PyVRP		✓	✓						✓	✓	✓	✓	✓
MDCVRPBPL	PyVRP		✓	✓						✓	✓	✓	✓	
MDOCVRPBPTW	PyVRP		✓	✓			✓	✓	✓	✓	✓	✓	✓	✓
MDCVRPBLTW	PyVRP		✓	✓			✓	✓	✓	✓	✓	✓	✓	
MDCVRPBTW	PyVRP		✓	✓			✓	✓	✓	✓	✓	✓	✓	
MDOCVRPBPL	PyVRP		✓	✓						✓	✓	✓	✓	✓
MDOCVRPBLTW	PyVRP		✓	✓			✓	✓	✓	✓	✓	✓	✓	✓
SPCTSP	ILS		✓		✓	✓				✓				

Table 8: The problem representations of 52 VRP variants that have not yet been explored in current literature. Here, RI represents the random identifier, and EAT, LAT, and ST indicate the earliest arrival time, the latest arrival time, and the service time, respectively.

Problem	Oracle	RI	Coord.	Demand	Prize	Penalty	EAT	LAT	ST	Depot	Pickup	Delivery	Sub-routes	Open Route
ACVRPTW	OR-Tools	✓		✓			✓	✓	✓	✓		✓	✓	
AOCVRP	OR-Tools	✓		✓						✓		✓	✓	✓
ACVRPL	OR-Tools	✓		✓						✓		✓	✓	
ACVRPB	OR-Tools	✓		✓						✓	✓	✓	✓	
AOCVRPTW	OR-Tools	✓		✓			✓	✓	✓	✓		✓	✓	✓
AOCVRPB	OR-Tools	✓		✓						✓	✓	✓	✓	✓
ACVRPBL	OR-Tools	✓		✓						✓	✓	✓	✓	
ACVRPLTW	OR-Tools	✓		✓			✓	✓	✓	✓		✓	✓	
AOCVRPBTW	OR-Tools	✓		✓			✓	✓	✓	✓	✓	✓	✓	✓
ACVRPBLTW	OR-Tools	✓		✓			✓	✓	✓	✓	✓	✓	✓	
AOCVRPL	OR-Tools	✓		✓						✓		✓	✓	✓
ACVRPBTW	OR-Tools	✓		✓			✓	✓	✓	✓	✓	✓	✓	
AOCVRPBL	OR-Tools	✓		✓						✓	✓	✓	✓	✓
AOCVRPLTW	OR-Tools	✓		✓			✓	✓	✓	✓		✓	✓	✓
AOCVRPBLTW	OR-Tools	✓		✓			✓	✓	✓	✓	✓	✓	✓	✓
ACVRPBP	OR-Tools	✓		✓						✓	✓	✓	✓	
AOCVRPBP	OR-Tools	✓		✓						✓	✓	✓	✓	✓
ACVRPBPL	OR-Tools	✓		✓						✓	✓	✓	✓	
AOCVRPBPTW	OR-Tools	✓		✓			✓	✓	✓	✓	✓	✓	✓	✓
ACVRPBLTW	OR-Tools	✓		✓			✓	✓	✓	✓	✓	✓	✓	
ACVRPBTW	OR-Tools	✓		✓			✓	✓	✓	✓	✓	✓	✓	
AOCVRPBPL	OR-Tools	✓		✓						✓	✓	✓	✓	✓
AOCVRPBLTW	OR-Tools	✓		✓			✓	✓	✓	✓	✓	✓	✓	✓
AMDCVRP	OR-Tools	✓		✓						✓		✓	✓	
AMDCVRPTW	OR-Tools	✓		✓			✓	✓	✓	✓		✓	✓	
AMDOCVRP	OR-Tools	✓		✓						✓		✓	✓	✓
AMDCVRPL	OR-Tools	✓		✓						✓		✓	✓	
AMDCVRPB	OR-Tools	✓		✓						✓	✓	✓	✓	
AMDOCVRPTW	OR-Tools	✓		✓			✓	✓	✓	✓		✓	✓	✓
AMDOCVRPB	OR-Tools	✓		✓						✓	✓	✓	✓	✓
AMDCVRPBL	OR-Tools	✓		✓						✓	✓	✓	✓	
AMDCVRPLTW	OR-Tools	✓		✓			✓	✓	✓	✓		✓	✓	
AMDOCVRPBTW	OR-Tools	✓		✓			✓	✓	✓	✓	✓	✓	✓	✓
AMDCVRPBLTW	OR-Tools	✓		✓			✓	✓	✓	✓	✓	✓	✓	
AMDOCVRPL	OR-Tools	✓		✓						✓		✓	✓	✓
AMDCVRPBTW	OR-Tools	✓		✓			✓	✓	✓	✓	✓	✓	✓	
AMDOCVRPBL	OR-Tools	✓		✓						✓	✓	✓	✓	✓
AMDOCVRPLTW	OR-Tools	✓		✓			✓	✓	✓	✓		✓	✓	✓
AMDOCVRPBLTW	OR-Tools	✓		✓			✓	✓	✓	✓	✓	✓	✓	✓
AMDCVRPBP	OR-Tools	✓		✓						✓	✓	✓	✓	
AMDOCVRPBP	OR-Tools	✓		✓						✓	✓	✓	✓	✓
AMDCVRPBPL	OR-Tools	✓		✓						✓	✓	✓	✓	
AMDOCVRPBPTW	OR-Tools	✓		✓			✓	✓	✓	✓	✓	✓	✓	✓
AMDCVRPBLTW	OR-Tools	✓		✓			✓	✓	✓	✓	✓	✓	✓	
AMDCVRPBTW	OR-Tools	✓		✓			✓	✓	✓	✓	✓	✓	✓	
AMDOCVRPBPL	OR-Tools	✓		✓						✓	✓	✓	✓	✓
AMDOCVRPBLTW	OR-Tools	✓		✓			✓	✓	✓	✓	✓	✓	✓	✓
APDTSP	OR-Tools	✓								✓	✓	✓		
PDCVRP	OR-Tools		✓	✓						✓	✓	✓	✓	
OPDCVRP	OR-Tools		✓	✓						✓	✓	✓	✓	✓
APDCVRP	OR-Tools	✓		✓						✓	✓	✓	✓	
AOPDCVRP	OR-Tools	✓		✓						✓	✓	✓	✓	✓

E Model Architecture and Training

E.1 Encoder

Similar to previous work (Kool et al., 2019; Kwon et al., 2020), we also use the encoder composed of L stacked attention layers, where each attention layer consists of two sub-layers: an attention sub-layer and a Feed-Forward (FF) sub-layer, both of which use Instance Normalization (Ulyanov et al., 2016) and skip-connection (He et al., 2016).

Let $H^{(\ell-1)} = \{\mathbf{h}_i^{(\ell-1)}\}_{i=0}^n$ denote the input to the ℓ-th attention layer for $\ell = 1, \ldots, L$. The outputs for the i-th node are computed as follows:

$$\widetilde{\mathbf{h}}_i^{(\ell)} = \mathrm{IN}^{(\ell)}\left(\mathbf{h}_i^{(\ell-1)} + \mathrm{MBM}^{(\ell)}\left(\mathbf{h}_i^{(\ell-1)}, H^{(\ell-1)}, \boldsymbol{D}, \boldsymbol{D}^{\mathrm{T}}, \boldsymbol{R}\right)\right), \tag{10}$$

$$\mathbf{h}_i^{(\ell)} = \mathrm{IN}^{(\ell)}\left(\widetilde{\mathbf{h}}_i^{(\ell)} + \mathrm{FF}^{(\ell)}\left(\widetilde{\mathbf{h}}_i^{(\ell)}\right)\right), \tag{11}$$

where $\mathrm{IN}(\cdot)$ denotes instance normalization (Ulyanov et al., 2016), MBM represents the adopted mixed bias module (see Equation (5) for details), and $\mathrm{FF}(\cdot)$ in Equation (11) corresponds to a fully connected neural network with ReLU activation.

After L attention layers, the final node embeddings $H^{(L)} = \{\mathbf{h}_i^{(L)}\}_{i=0}^n$ encapsulate the advanced feature representations of each node.

Notably, to ensure dimensional consistency across bias channels, we normalize $\boldsymbol{D}$ and $\boldsymbol{D}^{\mathbf{T}}$ by dividing their maximum value before passing the MBM.

E.2 Decoder

In URS, all parameters $\boldsymbol{\theta}_{dec}(\boldsymbol{\lambda})$ are adaptively generated conditioned on the multi-hot problem representation $\boldsymbol{\lambda}$ (see Appendix D for detailed problem representations). $\boldsymbol{\theta}_{dec}(\boldsymbol{\lambda})$ includes two MLP networks, which are $\mathrm{WEIGHT}(\boldsymbol{\lambda})$ and $\mathrm{BIAS}(\boldsymbol{\lambda})$. $\mathrm{WEIGHT}(\boldsymbol{\lambda})$ is used to generate linear projection matrices $[W_Q(\boldsymbol{\lambda}),\ W_K(\boldsymbol{\lambda}),\ W_V(\boldsymbol{\lambda})]$. $\mathrm{BIAS}(\boldsymbol{\lambda})$ in Equation (6) is used to generate bias weights for $\mathrm{Attention}(\cdot)$(see Equation (8)) and compatibility (see Equation (9)).

For $\mathrm{WEIGHT}(\boldsymbol{\lambda})$, we use a multi-layer MLP hypernetwork conditioned on a 13-dimensional problem representation $\boldsymbol{\lambda}$ to generate problem-specific adaptive parameters. Note that we factor $W_Q(\boldsymbol{\lambda}) \in \mathbb{R}^{(2d+1)\times d}$ into three vertically concatenated blocks $W_{\text{first}}(\boldsymbol{\lambda}) \in \mathbb{R}^{d\times d}, W_{\text{last}}(\boldsymbol{\lambda}) \in \mathbb{R}^{d\times d}$ and $W_C(\boldsymbol{\lambda}) \in \mathbb{R}^{1\times d}$, applied respectively to the first visited node $\mathbf{h}_{\pi_1}^{(L)}$, the last visited node $\mathbf{h}_{\pi_{t-1}}^{(L)}$, and a scalar state feature $C_t \in \mathbb{R}^1$ (see Appendix E.3 for more details). Thus $\mathrm{WEIGHT}(\boldsymbol{\lambda})$ outputs the linear projection matrices $\{W_{\text{first}}(\boldsymbol{\lambda}), W_{\text{last}}(\boldsymbol{\lambda}), W_C(\boldsymbol{\lambda}), W_K(\boldsymbol{\lambda}), W_V(\boldsymbol{\lambda})\}$.

Furthermore, we adopt the parameter compression technique of Ha et al. (2016) to control model size. Specifically, we first generate an advanced embedding matrix $\boldsymbol{H}_{\text{dec}}(\boldsymbol{\lambda}) = [\boldsymbol{h}_{\text{dec}}^i(\boldsymbol{\lambda}) | i = 1, 2, \ldots, 5] \in \mathbb{R}^{5\times|\boldsymbol{\lambda}|}$ whose five row embeddings each parameterize one target projection matrix. It can be computed via three consecutive linear projections:

$$\boldsymbol{H}_{\text{dec}}(\boldsymbol{\lambda}) = ((\boldsymbol{\lambda}W_1 + \mathbf{b}_1)W_2 + \mathbf{b}_2)W_3 + b_3, \tag{12}$$

where $W_1 \in \mathbb{R}^{|\lambda|\times d_h},\ W_2 \in \mathbb{R}^{d_h\times d_h},\ W_3 \in \mathbb{R}^{d_h\times(5\times|\boldsymbol{\lambda}|)},\ \mathbf{b}_1 \in \mathbb{R}^{d_h},\ \mathbf{b}_2 \in \mathbb{R}^{d_h}, \mathbf{b}_2 \in \mathbb{R}^{(5\times|\boldsymbol{\lambda}|)}$ are learnable parameters, d_h is 256 in this work, following Lin et al. (2022). Next, we use five different linear projections to map the new representation $\boldsymbol{h}_{\text{dec}}^i(\boldsymbol{\lambda})$ of each row to the corresponding decoder parameters. The computation can be expressed as:

$$W_{\text{first}}(\boldsymbol{\lambda}) = \boldsymbol{h}_{\text{dec}}^1(\boldsymbol{\lambda})W_{\textbf{hyper}}^1,\ W_{\text{last}}(\boldsymbol{\lambda}) = \boldsymbol{h}_{\text{dec}}^2(\boldsymbol{\lambda})W_{\textbf{hyper}}^2,\ W_C(\boldsymbol{\lambda}) = \boldsymbol{h}_{\text{dec}}^3(\boldsymbol{\lambda})W_{\textbf{hyper}}^3, \tag{13}$$

$$W_K(\boldsymbol{\lambda}) = \boldsymbol{h}_{\text{dec}}^4(\boldsymbol{\lambda})W_{\textbf{hyper}}^4,\ W_V(\boldsymbol{\lambda}) = \boldsymbol{h}_{\text{dec}}^5(\boldsymbol{\lambda})W_{\textbf{hyper}}^5, \tag{14}$$

where $W_{\textbf{hyper}}^1 \in \mathbb{R}^{|\lambda|\times(d\times d)}$, $W_{\textbf{hyper}}^2 \in \mathbb{R}^{|\lambda|\times(d\times d)}$, $W_{\textbf{hyper}}^3 \in \mathbb{R}^{|\lambda|\times(1\times d)}$, $W_{\textbf{hyper}}^4 \in \mathbb{R}^{|\lambda|\times(d\times d)}$, $W_{\textbf{hyper}}^5 \in \mathbb{R}^{|\lambda|\times(d\times d)}$ are learnable parameters. In this way, we use a simple MLP hypernetwork $\mathrm{WEIGHT}(\boldsymbol{\lambda})$ to generate used linear projection matrices $\{W_Q(\boldsymbol{\lambda}),\ W_K(\boldsymbol{\lambda}),\ W_V(\boldsymbol{\lambda})\}$ conditioned on the multi-hot problem representation $\boldsymbol{\lambda}$, enabling the adaptive construction of high-quality solutions for different problems.

E.3 PROBLEM STATE C_t

In this section, we detail the problems that require additional state signals. If a problem is not mentioned in this section, it means we will not apply any extra state to it, i.e., $C_t = 0$.

For all problems with the capacity constraint, we explicitly impose **only remaining load**, while diverse additional constraints (e.g., time windows, duration limit, and backhaul) are enforced implicitly as $\mathcal{M}_t$ masks infeasible candidate nodes to guarantee valid solutions, instead of being fully enumerated in the input of the decoder.

For OP, we keep track of the remaining maximum length at time t, and C_t represents the remaining routing length that can be moved, and we normalize it to $[0, 1]$ by dividing by the maximum length (i.e., 4.0 in OP100). The setting is the same as AM (Kool et al., 2019).

For PCTSP and SPCTSP, C_t is the remaining prize to collect, and we do not provide any information about the penalties, as this is irrelevant for the remaining decisions, following Kool et al. (2019).

For the problem state, we provide an ablation study in Appendix K.2.

E.4 TRAINING

Following Kwon et al. (2020), we use n trajectories with distinct starting nodes in training. URS is trained by the REINFORCE (Williams, 1992) algorithm with a shared baseline (Kwon et al., 2020):

$$\nabla_\theta \mathcal{L}(\boldsymbol{\theta}) = \mathbb{E}_{p(\boldsymbol{\pi}|\mathcal{G},\boldsymbol{\theta})}[(f(\boldsymbol{\pi}|\mathcal{G}) - \frac{1}{n}\sum_{i=1}^{n} f(\boldsymbol{\pi}^i|\mathcal{G}))\nabla_{\boldsymbol{\theta}} \log p_{\boldsymbol{\theta}}(\boldsymbol{\pi}|\mathcal{G})], \tag{15}$$

$$p_{\boldsymbol{\theta}}(\boldsymbol{\pi} \mid \mathcal{G}) = \prod_{t=2}^{n} p_{\boldsymbol{\theta}}(\pi_t \mid \mathcal{G}, \pi_{1:t-1}), \tag{16}$$

where the objective function $f(\boldsymbol{\pi}|\mathcal{G})$ represents the total reward (e.g., the negative value of tour length) of instance $\mathcal{G}$ given a specific solution $\boldsymbol{\pi}$.

F ADAPTATION ATTENTION FREE MODULE

Following Zhou et al. (2024a), we implement $\mathrm{Attention}(\cdot)$ using an adaptation attention free module (AAFM) to enhance geometric pattern recognition for routing problems. Given the input X, AAFM first transforms it into Q, K, and V through corresponding linear projection operations:

$$Q = XW^Q, \quad K = XW^K, \quad V = XW^V, \tag{17}$$

where W^Q, W^K, and W^V are learnable matrices. The AAFM computation is then expressed as:

$$\mathrm{Attention}(Q, K, V, A) = \sigma(Q) \odot \frac{\exp(A)(\exp(K) \odot V)}{\exp(A)\exp(K)}, \tag{18}$$

where σ denotes the sigmoid function, $\odot$ represents the element-wise product, and $A = \{a_{ij}\}$ denotes the pair-wise adaptation bias. For distance matrices, the corresponding adaptation bias $f(\alpha, N, d_{ij}) = -\alpha \cdot \log_2 N \cdot d_{i,j}$. Here, N denotes the total number of nodes (i.e., problem size), and α is generated via a lightweight network $\mathrm{BIAS}(\boldsymbol{\lambda})$ in our paper (see Equation (6)). Notably, for the relation matrix, we remove the scale N in the calculation of adaptation bias because the relation is scale-independent.

Compared to multi-head attention (MHA) (Vaswani et al., 2017), AAFM enables the model to explicitly capture instance-specific knowledge by updating pair-wise adaptation biases while exhibiting lower computational overhead. Further details are provided in the related work section mentioned above.

G LLM-DRIVEN CONSTRAINT SATISFACTION MECHANISM

To operationalize the UDR framework for a vast spectrum of routing problems, we introduce an automated constraint satisfaction mechanism based on LLMs. This mechanism obviates the need for manual, problem-specific masks by automatically designing executable **mask generators**. This approach follows the generate-and-validate pipeline, transforming constraint specifications into reliable code.

G.1 MASK GENERATOR DESIGN

This process begins by prompting an LLM with a prompt that comprises two key elements: 1) a natural language **task description** requires explicit and precise specification of both the optimization objective for the task and all associated operational constraints, as this component delineates the core problem to resolve; and 2) a standardized Python **code template** formally defines the environment by outlining the precise semantics, shapes, and data types of all input and output tensors, thereby specifying how the solution should interface with the existing code.

Our generation process relies on the clarity and accuracy of these components. When the problem is well-posed with clear objectives and precise I/O, the mask generator design process is highly efficient. Conversely, failures usually result from incomplete or ambiguous specification of the core components, not minor phrasing variations.

Here is an example for generating a mask for the CVRPTW that enforces constraints: 1) no revisiting nodes except the depot, 2) no exceeding current vehicle capacity, 3) arrival before node time windows, 4) only the depot being revisitable, and 5) no consecutive depot visits unless all other nodes are visited.

Task Description: Given the current node, visited nodes, coordinates, demands, service times, available time windows, current capacity, current time, and the number of nodes, design a function to mask nodes that are either already visited, have demands exceeding capacity, or cannot be reached before their time window closed, considering the travel time from the current node (where travel time equals distance due to unit speed) plus the required service time at that node. Only the depot may be visited more than once. However, you can't visit the depot twice in a row unless all other nodes have already been visited.

Code Template:

```
import torch
def mask_illegal_nodes(current_node: torch.Tensor, visited_nodes: torch.Tensor, coordinates: torch.Tensor,
                       demands: torch.Tensor, service_time: torch.Tensor, time_windows: torch.Tensor,
                       current_capacity: torch.Tensor, current_time: torch.Tensor, num_nodes: int) -> torch.Tensor:
    """
    Design a function to mask nodes that are either already visited, have demands exceeding capacity, or cannot be reached within their time window in each step.
    The operation processes batches in parallel, so no loops over the batch dimension are allowed-inputs must use batch-first shapes.

    Args:
    current_node: ID of the current node. Shape: [batch_size, 1]
    visited_nodes: Array of IDs of visited nodes and depot. Shape: [batch_size, num_visited_nodes]
    coordinates: Coordinates of the deopt and all nodes. Shape: [batch_size, num_nodes+1, 2]
    demands: Array of demands of the deopt and all nodes. Shape: [batch_size, num_nodes+1]
    service_time: Array of service time of the deopt and all nodes. Shape: [batch_size, num_nodes+1]
    time_windows: Array of available time window of the deopt and all nodes. Shape: [batch_size, num_nodes+1, 2]
```

```
    current_capacity: Value of current capacity. Shape: [batch_size, 1]
    current_time: Value of current time. Shape: [batch_size, 1]
    num_nodes: The number of nodes.

    Return:
    mask: Boolean mask indicating valid deopt or nodes (True = selectable, False = masked). Shape: [batch_size, num_nodes+1]
    """
    return mask
```

The LLM completes the function body with the prompt guidance. The candidate mask generator is an executable Python snippet implementing the described logic:

```
def mask_illegal_nodes(current_node: torch.Tensor, visited_nodes: torch.Tensor, coordinates: torch.Tensor, demands: torch.Tensor, service_time: torch.Tensor, time_windows: torch.Tensor, current_capacity: torch.Tensor, current_time: torch.Tensor, num_nodes: int) -> torch.Tensor:
    """
    Design a function to mask nodes that are either already visited, have demands exceeding capacity, or cannot be reached within their time window in each step.
    The operation processes batches in parallel, so no loops over the batch dimension are allowed\u2014inputs must use batch-first shapes.
    Args:
    current_node: ID of the current node. Shape: [batch_size, 1]
    visited_nodes: Array of IDs of visited nodes and depot. Shape: [batch_size, num_visited_nodes]
    coordinates: Coordinates of the deopt and all nodes. Shape: [batch_size, num_nodes+1, 2]
    demands: Array of demands of the deopt and all nodes. Shape: [batch_size, num_nodes+1]
    service_time: Array of service time of the deopt and all nodes. Shape: [batch_size, num_nodes+1]
    time_windows: Array of available time window of the deopt and all nodes. Shape: [batch_size, num_nodes+1, 2]
    current_capacity: Value of current capacity. Shape: [batch_size, 1]
    current_time: Value of current time. Shape: [batch_size, 1]
    num_nodes: The number of nodes.
    Return:
    mask: Boolean mask indicating valid deopt or nodes (True = selectable, False = masked). Shape: [batch_size, num_nodes+1]
    """
    batch_size = current_node.size(0)
    device = current_node.device
    # Shape helpers
    N = num_nodes + 1  # Including depot at idx 0
    # 1) Mask already visited nodes (except depot handled later)
    # Create visited mask: True if visited, False otherwise
    visited_mask = torch.zeros((batch_size, N), dtype=torch.bool, device=device)
    # visited_nodes: [batch_size, num_visited_nodes], scatter True for each node visited
    # Use one-hot scatter add to build visited_mask
    idx = visited_nodes.unsqueeze(-1)  # [batch_size, num_visited_nodes, 1]
    # For scatter we reshape visited_mask to 1D first per batch later
    # Instead do scatter_ at dim=1
    visited_mask = visited_mask.scatter_(1, visited_nodes, True)
    # 2) Mask nodes with demands exceeding capacity
    # demands: [batch_size, N], current_capacity: [batch_size,1]
    demand_mask = demands <= current_capacity  # True if demand <= capacity
    # 3) Mask nodes that cannot be reached within their time window
```

```
    # Calculate travel time = Euclidean distance current_node -> all nodes
    # coordinates: [batch_size, N, 2]
    # current_node: [batch_size, 1]
    current_coords = torch.gather(coordinates, 1, current_node.unsqueeze(-1).expand(-1, -1, 2)).squeeze(1)  # [batch_size, 2]
    # All nodes coords: coordinates [batch_size, N, 2]
    # Compute distance = Euclidean norm
    diff = coordinates - current_coords.unsqueeze(1)  # [batch_size, N, 2]
    travel_time = diff.norm(dim=2)  # [batch_size, N]
    # Arrival time at each candidate node (without waiting): current_time + travel_time
    arrival_time = current_time + travel_time  # [batch_size, N]
    # Time windows: [batch_size, N, 2]
    window_start = time_windows[..., 0]
    window_end = time_windows[..., 1]
    # We can arrive early but must wait for window start if arrival_time < window_start
    start_service_time = torch.max(arrival_time, window_start)  # [batch_size, N]
    # Departure time from node = start_service_time + service_time
    departure_time = start_service_time + service_time  # [batch_size, N]
    # Node feasible if arrival_time <= window_end (i.e., can start service before window closes)
    time_mask = arrival_time <= window_end  # can arrive on time to start service
    # 4) Mask depot revisits constraints:
    # Depot is node 0
    depot_idx = torch.zeros(batch_size, dtype=torch.long, device=device)
    # Check if current_node == depot (node 0) to mask depot twice in a row
    current_is_depot = (current_node.squeeze(1) == 0)  # [batch_size]
    # Check if all other nodes are visited (excluding depot)
    # visited_mask: True for visited nodes incl depot
    # Count number of visited non-depot nodes:
    visited_non_depot = visited_mask[:, 1:]  # [batch_size, N-1]
    all_others_visited = visited_non_depot.all(dim=1)  # [batch_size]
    # Mask depot if current node is depot and last visited node is depot (i.e., depot twice in a row)
    # but allow depot if all other nodes have been visited
    # So depot_masked_forbidden = True if depot is forbidden, False if allowed
    # By problem statement: \"Only the depot may be visited multiple times. However, you can\u2019t visit the depot twice in a row unless all other nodes have already been visited.\"
    # Check if previous node == depot (as we have current_node only, we assume last visit is current_node)
    # So if current_node == depot and next node is also depot, it is forbidden unless all other have been visited
    # Initially depot_mask lets depot be selected
    depot_mask = torch.ones((batch_size,), dtype=torch.bool, device=device)
    # If current node is depot and not all others visited => mask depot = False (mask it)
    mask_depot = current_is_depot & (~all_others_visited)  # batches where depot revisit is forbidden
    depot_mask[mask_depot] = False  # mask depot for these batches
    # Build full mask of depot for all batches:
    # depot_mask shape: [batch_size], need to broadcast to [batch_size, N]
    # depot_mask[:, None] for expand
    depot_mask_full = torch.ones((batch_size, N), dtype=torch.bool, device=device)
    depot_mask_full[:, 0] = depot_mask  # depot node mask per batch
```

```
    # 5) Depot can be visited more than once, so remove depot from visited_mask
    visited_mask[:, 0] = False  # depot can be visited multiple times (masking will depend on depot_mask)
    # Combine all masks
    # True = selectable, False = masked
    final_mask = (~visited_mask) & demand_mask & time_mask & depot_mask_full
    return final_mask
```

G.2 Automated Validation

Each candidate generator is then validated. We execute it within the URS solver or a simple simulated solver on a set of problem instances and use a problem-specific **checker** function to verify if the resulting solutions are constraint-compliant. For the CVRPTW example, the checker validates fundamental feasibility constraints, including capacity limits, time window adherence, and unique customer visitation. The restriction on consecutive depot visits is excluded from validation, serving instead as a mechanism to prevent algorithmic stagnation.

```
import torch

def cvrptw_checker(env, solutions):
    batch_size, num_steps = solutions.shape
    # all nodes visited once
    all_nodes_visited = (torch.arange(env.problem_size + 1).unsqueeze(0).expand(batch_size, -1) == sorted[:, -env.problem_size - 1:]).all(1)
    if not all_nodes_visited.any():
        return -float('inf')
    for i in range(num_steps):
        crt_state = env.update(solutions[:, i])
        # time window
        if (env.current_time > crt_state.selected_time[:, -1]).any():
            return -float('inf')
        # capacity
        if (env.available_capacity < crt_state.selected_demand).any():
            return -float('inf')
    return -1.0
```

G.3 AHD Framework Integration

For most common VRP variants, manually writing a masking function for each problem is possible by decoupling constraints. However, it is fundamentally more challenging than writing a post-hoc checker. While a checker simply validates a static, completed solution, a masking function must proactively guarantee feasibility by determining whether a current action would render the future route infeasible. Even if constraints can be checked individually, implementing this look-ahead logic correctly and efficiently is not a trivial task, which requires significant domain expertise for each constraint. Our mechanism automates this manual engineering task for the vast majority of variants, thereby lowering the barrier for users.

In our proposed framework, each masking function is validated by a problem-specific checker on a set of test instances. Finding the valid masking function is an offline generate-and-validate process, rather than relying on an LLM to perform online reasoning during the inference phase of the neural solver. We leverage automatic heuristic design frameworks (such as EoH Liu et al. (2024b)) to enable the LLM to iteratively refine the code of the masking function based on the checker's feedback. Any candidate masking function that produces even one infeasible solution in the test instances (i.e., validity rate $< 100\%$) is discarded. Once a valid masking function is obtained, it is used in the subsequent NCO process, and the offline process is terminated. In other words, every final valid masking function produced by the LLM is reliable, and it will generate valid masks for each solution construction step of the NCO process. The cost of the offline process is a one-time amortized cost per problem variant, as the generated masking function can be reused indefinitely for any instance of that variant.

G.4 Consistency Across Different LLMs

To evaluate the influence of our framework on different LLMs, we benchmarked its performance using both GPT-3.5-turbo and GPT-4o-mini. The results, presented in Table 9 and Table 10, show that while the query efficiency varies with the underlying model's capability, the core outcome remains consistent: our framework successfully generates the necessary masking functions with both models. This finding demonstrates that our approach doesn't rely on a specific proprietary model but rather provides a robust methodology adaptable to various powerful LLMs.

Table 9: Cost analysis of generating mask functions for 11 training tasks using GPT-3.5-turbo.

	ATSP	TSP	OP	PCTSP	PDTSP	OCVRPTW
#Query	1	1	1	4	1	5
#Token	468	514	1359	3403	1277	11054
Time	<1min	<1min	<1min	1min	<1min	1min
	ACVRP	**CVRP**	**CVRPTW**	**CVRPB**	**OCVRP**	**Avg.**
#Query	1	1	5	2	1	2
#Token	1253	1371	9935	1920	1264	3074
Time	<1min	<1min	<1min	<1min	<1min	<1min

Table 10: Cost analysis of generating mask functions for 11 training tasks using GPT-4o-mini.

	ATSP	TSP	OP	PCTSP	PDTSP	OCVRPTW
#Query	1	1	3	1	10	17
#Token	459	387	2031	650	9877	18031
Time	<1min	<1min	<1min	<1min	2min	3min
	ACVRP	**CVRP**	**CVRPTW**	**CVRPB**	**OCVRP**	**Avg.**
#Query	1	1	15	3	2	5
#Token	1273	1245	15103	1920	1264	4749
Time	<1min	<1min	3min	<1min	<1min	1min

H Training and Model Settings

H.1 Multi-Task Version

The detailed information about the hyperparameter settings can be found in Table 11. The training of URS is conducted on a single NVIDIA GeForce RTX 4090 GPU (24GB memory). The training procedure requires only about 95 hours ($\approx$ 4 days) in total (500 epochs at approximately 12 minutes each) to obtain a unified parameter set capable of addressing a broad class of routing problems.

H.2 Single-Task Version

URS-STL is trained on data from only a single problem type (e.g., "URS-STL (CVRP)" is trained only on CVRP). The URS-STL variant uses exactly the same model architecture, hyperparameters (e.g., embedding dimension, number of layers, optimizer), and training setup (e.g., initial learning rate, batch size) as the multi-task URS described in Section 5.1 and Appendix H.1. The only modification we made is to the training duration. We observed that the single-task models converge significantly faster than the multi-task model. Therefore, we train URS-STL models for 300 epochs, with a learning rate decay applied at the 251st epoch. This contrasts with the multi-task URS, which is trained for 500 epochs with decay applied at the 451st epoch. This adjustment is made solely to reflect the faster convergence of the single-task training. All other hyperparameters and model architecture remain identical.

Table 11: The hyperparameter settings of URS.

Hyperparameter	Value
Optimizer	AdamW
Clipping parameter ζ	50
Initial learning rate	10^{-4}
Epochs of learning rate decay	[451]
Factor of learning rate decay	0.1
Weight decay	10^{-6}
The number of encoder layers L	12
Embedding dimension d	128
Feed forward dimension	512
Dimension d_h in Equation (12)	256
Training scale	100
Batches of each epoch	$2,000$
Batch size	128
Training Epochs	500

I GENERALIZATION TO UNSEEN VRPS

To comprehensively evaluate zero-shot generalization of URS, we test its performance on a diverse set of 96 unseen problems. This set is designed to cover both established and novel challenges, including 44 well-studied VRP variants from the NCO literature and 52 newly introduced variants that have not been explored before. The detailed results are presented in Table 12 and Table 13. On widely-studied constraints (i.e., C, O, L, TW, MD, B, BP), URS continues to deliver high-quality solutions. Notably, URS merely selects the next node from a given feasible candidates without any additional domain knowledge, making its performance especially meaningful. Benefiting from our UDR, URS can directly address previously unexplored variants, which compound asymmetry and PD relations. Without any fine-tuning, URS still constructs high-quality solutions for them, strengthening the broad problem generality and deployment efficiency.

Table 12: Zero-shot generalization performance across 44 VRP variants that have been explored in current literature (Liu et al., 2024a; Berto et al., 2024) ($N = 100$).

Method	CVRPBP		OCVRPBP		CVRPBPL		OCVRPBPTW		CVRPBPLTW	
	Gap	Time	Gap	Time	Gap	Time	Gap	Time	Gap	Time
Oracle Solver	0.00%	6.6m	0.00%	6.6m	0.00%	6.6m	0.00%	6.6m	0.00%	6.6m
MVMoE	13.95%	14s	17.36%	14s	13.38%	14s	2.29%	15s	10.46%	16s
MTPOMO	13.71%	7s	16.94%	8s	13.44%	8s	3.26%	9s	11.35%	10s
ReLD-MTL	13.57%	9s	14.83%	9s	12.96%	10s	2.27%	11s	10.80%	12s
URS	**12.95%**	7s	**14.30%**	7s	**12.65%**	8s	**-3.47%**	8s	**9.74%**	10s

Method	CVRPBPTW		OCVRPBPL		OCVRPBPLTW		CVRPL		CVRPBL	
	Gap	Time	Gap	Time	Gap	Time	Gap	Time	Gap	Time
Oracle Solver	0.00%	6.6m	0.00%	6.6m	0.00%	6.6m	0.00%	16m	0.00%	3.5h
MVMoE	10.85%	15s	16.88%	14s	1.84%	16s	0.26%	12s	1.35%	12s
MTPOMO	11.53%	9s	16.39%	8s	2.77%	10s	0.48%	6s	1.79%	6s
ReLD-MTL	11.07%	11s	14.22%	10s	1.79%	11s	**0.02%**	8s	**1.01%**	7s
URS	**9.73%**	9s	**13.81%**	8s	**-3.77%**	9s	0.43%	7s	1.65%	6s

Method	OCVRPB		CVRPLTW		OCVRPBTW		CVRPBLTW		OCVRPL	
	Gap	Time	Gap	Time	Gap	Time	Gap	Time	Gap	Time
Oracle Solver	0.00%	3.5h	0.00%	3.5h	0.00%	3.5h	0.00%	3.5h	0.00%	3.5h
MVMoE	7.09%	12s	1.47%	16s	9.95%	15s	7.33%	16s	3.15%	13s
MTPOMO	7.34%	5s	1.92%	9s	10.45%	6s	7.75%	8s	3.44%	6s
ReLD-MTL	**5.36%**	6s	**1.17%**	11s	**9.29%**	8s	**6.94%**	9s	**2.31%**	8s
URS	9.35%	6s	2.67%	9s	13.77%	7s	9.18%	8s	3.22%	7s

Method	CVRPBTW		OCVRPBL		OCVRPLTW		OCVRPBLTW		MDCVRPBP	
	Gap	Time	Gap	Time	Gap	Time	Gap	Time	Gap	Time
Oracle Solver	0.00%	3.5h	0.00%	3.5h	0.00%	3.5h	0.00%	3.5h	0.00%	6.6m
MVMoE	7.08%	15s	7.12%	12s	3.90%	15s	10.01%	15s	64.91%	33s
MTPOMO	7.41%	7s	7.34%	7s	4.37%	8s	10.50%	7s	45.66%	24s
ReLD-MTL	**6.74%**	8s	**5.41%**	7s	**3.16%**	9s	**9.22%**	8s	40.28%	27s
URS	8.94%	8s	9.47%	7s	5.12%	9s	13.72%	8s	**34.91%**	24s

Method	MDOCVRPBP		MDCVRPBPL		MDOCVRPBPTW		MDCVRPBPLTW		MDCVRPBPTW	
	Gap	Time	Gap	Time	Gap	Time	Gap	Time	Gap	Time
Oracle Solver	0.00%	6.6m	0.00%	6.6m	0.00%	6.6m	0.00%	6.6m	0.00%	6.6m
MVMoE	52.16%	33s	64.79%	36s	46.18%	38s	54.23%	42s	54.76%	39s
MTPOMO	40.15%	24s	45.84%	26s	34.19%	29s	40.26%	32s	40.32%	30s
ReLD-MTL	34.53%	27s	39.06%	29s	34.08%	34s	36.59%	37s	37.16%	35s
URS	**19.13%**	22s	**34.49%**	26s	**11.17%**	26s	**25.57%**	32s	**25.77%**	30s

Method	MDOCVRPBPL		MDOCVRPBPLTW		MDCVRP		MDCVRPTW		MDOCVRP	
	Gap	Time	Gap	Time	Gap	Time	Gap	Time	Gap	Time
Oracle Solver	0.00%	6.6m	0.00%	6.6m	0.00%	6.6m	0.00%	6.6m	0.00%	6.6m
MVMoE	51.72%	34s	45.23%	40s	31.90%	31s	53.64%	41s	29.08%	31s
MTPOMO	39.34%	27s	33.37%	32s	23.75%	23s	36.10%	31s	27.46%	23s
ReLD-MTL	34.48%	29s	33.83%	36s	17.37%	25s	**30.90%**	34s	22.32%	25s
URS	**18.90%**	24s	**10.96%**	28s	**9.65%**	23s	37.26%	32s	**22.01%**	23s

Method	MDCVRPL		MDCVRPB		MDOCVRPTW		MDOCVRPB		MDCVRPBL	
	Gap	Time	Gap	Time	Gap	Time	Gap	Time	Gap	Time
Oracle Solver	0.00%	6.6m	0.00%	6.6m	0.00%	6.6m	0.00%	6.6m	0.00%	6.6m
MVMoE	33.42%	34s	21.70%	26s	51.57%	40s	28.21%	26s	20.35%	29s
MTPOMO	24.32%	25s	12.89%	19s	35.71%	29s	25.06%	20s	11.10%	20s
ReLD-MTL	18.48%	28s	**9.38%**	21s	33.55%	33s	18.50%	21s	**8.26%**	23s
URS	**15.32%**	26s	13.14%	19s	**26.05%**	25s	**15.17%**	18s	11.19%	21s

Method	MDCVRPLTW		MDOCVRPBTW		MDCVRPBLTW		MDOCVRPL		MDCVRPBTW	
	Gap	Time	Gap	Time	Gap	Time	Gap	Time	Gap	Time
Oracle Solver	0.00%	6.6m	0.00%	6.6m	0.00%	6.6m	0.00%	6.6m	0.00%	6.6m
MVMoE	55.55%	44s	62.47%	35s	63.18%	37s	29.33%	33s	65.90%	35s
MTPOMO	37.34%	32s	45.55%	25s	45.07%	27s	27.21%	25s	45.94%	25s
ReLD-MTL	**31.56%**	36s	43.36%	28s	40.57%	30s	**22.05%**	27s	41.28%	28s
URS	38.04%	35s	**30.32%**	22s	**37.70%**	27s	22.15%	25s	**37.78%**	25s

Method	MDOCVRPBL		MDOCVRPLTW		MDOCVRPBLTW		SPCTSP		–	
	Gap	Time	Gap	Time	Gap	Time	Gap	Time		
Oracle Solver	0.00%	6.6m	0.00%	6.6m	0.00%	6.6m	0.00%	1.6h	–	
MVMoE	28.70%	28s	51.09%	43s	62.10%	37s	–		–	
MTPOMO	25.01%	21s	35.39%	31s	45.48%	27s	–		–	
ReLD-MTL	18.50%	22s	33.26%	35s	43.27%	30s	–		–	
AM	–		–		–		2.69%	5s	–	
URS	**14.90%**	20s	**25.59%**	27s	**30.41%**	24s	**-2.37%**	5s	–	

Table 13: Zero-shot generalization performance across 52 VRP variants that have not yet been explored in the current literature ($N = 100$).

Method	ACVRPL		ACVRPBL		ACVRPLTW		ACVRPBLTW		AOCVRPL	
	Gap	Time	Gap	Time	Gap	Time	Gap	Time	Gap	Time
Oracle Solver	0.00%	6.6m	0.00%	6.6m	0.00%	6.6m	0.00%	6.6m	0.00%	6.6m
URS	**-2.24%**	1.9m	**6.18%**	2.4m	**12.22%**	2.7m	**10.18%**	2.4m	**37.36%**	3.1m

Method	AOCVRPBL		AOCVRPLTW		AOCVRPBLTW		ACVRPBPL		ACVRPBPLTW	
	Gap	Time	Gap	Time	Gap	Time	Gap	Time	Gap	Time
Oracle Solver	0.00%	6.6m	0.00%	6.6m	0.00%	6.6m	0.00%	6.6m	0.00%	6.6m
URS	**17.23%**	2.7m	**16.35%**	2.8m	**14.32%**	2.5m	**21.69%**	2.6m	**-0.58%**	2.8m

Method	AOCVRPBPL		AOCVRPBPLTW		ACVRPB		ACVRPTW		AOCVRP	
	Gap	Time	Gap	Time	Gap	Time	Gap	Time	Gap	Time
Oracle Solver	0.00%	6.6m	0.00%	6.6m	0.00%	6.6m	0.00%	6.6m	0.00%	6.6m
URS	**28.25%**	2.7m	**2.54%**	2.7m	**7.10%**	2.1m	**11.28%**	2.5m	**37.63%**	2.9m

Method	AOCVRPTW		AOCVRPB		AOCVRPBTW		ACVRPBTW		ACVRPBP	
	Gap	Time	Gap	Time	Gap	Time	Gap	Time	Gap	Time
Oracle Solver	0.00%	6.6m	0.00%	6.6m	0.00%	6.6m	0.00%	6.6m	0.00%	6.6m
URS	**17.47%**	2.6m	**18.05%**	2.5m	**14.45%**	2.3m	**9.95%**	2.2m	**21.94%**	2.4m

Method	AOCVRPBP		AOCVRPBPTW		ACVRPBPTW		APDTSP		AMDCVRPL	
	Gap	Time	Gap	Time	Gap	Time	Gap	Time	Gap	Time
Oracle Solver	0.00%	6.6m	0.00%	6.6m	0.00%	6.6m	0.00%	6.6m	0.00%	6.6m
URS	**28.27%**	2.5m	**3.28%**	2.5m	**0.12%**	2.6m	**6.21%**	1m	**7.15%**	6.1m

Method	AMDCVRPBL		AMDCVRPLTW		AMDCVRPBLTW		AMDOCVRPL		AMDOCVRPBL	
	Gap	Time	Gap	Time	Gap	Time	Gap	Time	Gap	Time
Oracle Solver	0.00%	6.6m	0.00%	6.6m	0.00%	6.6m	0.00%	6.6m	0.00%	6.6m
URS	**17.51%**	6.5m	**19.98%**	8.8m	**16.73%**	7.5m	**47.80%**	8.6m	**27.23%**	7.1m

Method	AMDOCVRPLTW		AMDOCVRPBLTW		AMDCVRPBPL		AMDCVRPBPLTW		AMDOCVRPBPL	
	Gap	Time	Gap	Time	Gap	Time	Gap	Time	Gap	Time
Oracle Solver	0.00%	6.6m	0.00%	6.6m	0.00%	6.6m	0.00%	6.6m	0.00%	6.6m
URS	**24.90%**	7.9m	**22.84%**	6.7m	**29.07%**	7.2m	**4.45%**	8.3m	**29.30%**	7.3m

Method	AMDOCVRPBPLTW		AMDCVRP		AMDCVRPTW		AMDOCVRP		AMDCVRPB	
	Gap	Time	Gap	Time	Gap	Time	Gap	Time	Gap	Time
Oracle Solver	0.00%	6.6m	0.00%	6.6m	0.00%	6.6m	0.00%	6.6m	0.00%	6.6m
URS	**8.63%**	7.5m	**3.56%**	5.3m	**20.96%**	8.1m	**48.02%**	7.8m	**17.35%**	5.8m

Method	AMDOCVRPTW		AMDOCVRPB		AMDOCVRPBTW		AMDCVRPBTW		AMDCVRPBP	
	Gap	Time	Gap	Time	Gap	Time	Gap	Time	Gap	Time
Oracle Solver	0.00%	6.6m	0.00%	6.6m	0.00%	6.6m	0.00%	6.6m	0.00%	6.6m
URS	**26.02%**	7.3m	**27.78%**	6.5m	**23.67%**	6.2m	**17.52%**	6.8m	**30.15%**	6.5m

Method	AMDOCVRPBP		AMDOCVRPBPTW		AMDCVRPBPTW		PDCVRP		OPDCVRP	
	Gap	Time	Gap	Time	Gap	Time	Gap	Time	Gap	Time
Oracle Solver	0.00%	6.6m	0.00%	6.6m	0.00%	6.6m	0.00%	6.6m	0.00%	6.6m
URS	**29.80%**	6.7m	**9.61%**	6.9m	**4.63%**	7.6m	**-1.47%**	4.3s	**4.93%**	4.3s

Method	APDCVRP		AOPDCVRP		–		–		–	
	Gap	Time	Gap	Time						
Oracle Solver	0.00%	6.6m	0.00%	6.6m	–		–		–	
URS	**7.03%**	1.2m	**11.13%**	1.2m	–		–		–	

J More Experiments

J.1 Training Problem Selection

As shown in Table 6, our selection of the 11 training problems is guided by a "minimum redundancy" principle: we ensure that most attributes in UDR appeared in at least two distinct problem types during training, which helps prevent the model from overfitting a specific attribute to a single problem. The only exception is the Penalty attribute, as preliminary experiments have shown that exposure in a single problem type is sufficient for generalization to variants such as PCTSP and SPCTSP.

To empirically validate this selection strategy, we train two additional variants and compare them with our original URS: URS-Diff (Different Selection) and URS-Expand (Broader Problems). The first variant, URS-Diff, uses a different problem set where OCVRPTW is replaced by attribute-independent CVRPL. This modification means that the Open Route and Time Window attributes each appear in only one training problem. The second variant, URS-Expand, is trained on a broader set of 22 problems, incorporating all variants evaluated in MTPOMO (Liu et al., 2024a) and MVMoE (Zhou et al., 2024b).

As shown in Table 14, URS-Diff performs significantly worse on unseen problems involving Open Route and Time Window constraints. Meanwhile, URS-Expand achieves a slightly better performance than URS due to seeing more problem variants during training. However, the original URS remains highly competitive. Remarkably, despite being trained on only half the number of problem types (11 vs. 22), URS achieves the best solution on 12 out of the 22 evaluated problems.

These results demonstrate that the choice of our selected 11 problems offers a balanced trade-off, providing sufficient attribute coverage for strong generalization while maintaining training efficiency. Expanding the training set yields only marginal gains, while a poorly selected set leads to poor cross-problem generalization. In future work, we plan to explore more effective training problem selection strategies to further enhance model performance and training efficiency.

Table 14: Comparison under different training problem settings. The symbol * indicates the original problem selection, and Δ represents a different problem selection of equal number. All test problems are encompassed within URS-Expand.

Method	ATSP (* Δ)	TSP(* Δ)	OP(* Δ)	PCTSP(* Δ)	PDTSP(* Δ)	ACVRP(*Δ)
URS-Diff	4.52%	1.05%	0.82%	1.31%	6.09%	5.10%
URS-Expand	4.77%	0.93%	0.99%	1.41%	5.85%	5.48%
URS	**2.26%**	**0.57%**	**0.45%**	**1.06%**	**4.98%**	**3.06%**
	CVRP(* Δ)	CVRPTW(* Δ)	CVRPB(* Δ)	OCVRP(* Δ)	OCVRPTW(*)	CVRPL(Δ)
URS-Diff	1.97%	6.26%	1.80%	3.75%	15.45%	0.58%
URS-Expand	2.04%	**5.62%**	1.77%	3.45%	**4.34%**	0.65%
URS	**1.81%**	6.13%	**1.46%**	**3.24%**	5.07%	**0.43%**
	OCVRPB	CVRPBL	CVRPLTW	OCVRPBTW	CVRPBLTW	OCVRPL
URS-Diff	7.55%	2.02%	2.76%	27.48%	10.25%	3.73%
URS-Expand	**5.39%**	1.88%	**2.03%**	**9.13%**	**6.29%**	3.41%
URS	9.35%	**1.65%**	2.67%	13.77%	9.18%	**3.22%**
	CVRPBTW	OCVRPBL	OCVRPLTW	OCVRPBLTW	Avg.gap	Best Sol.
URS-Diff	10.00%	7.56%	15.61%	27.80%	7.43%	0/22
URS-Expand	**6.07%**	**5.47%**	**4.38%**	**9.23%**	**4.12%**	10/22
URS	8.94%	9.47%	5.12%	13.72%	4.89%	**12/22**

J.2 Results on Different Evaluation Scenarios

Verifying performance under different evaluation scenarios is important for testing a model. To address this, we conducted a systematic evaluation using the exact scenarios from Sym-NCO (Kim et al., 2022). We utilize the test datasets directly from the official Sym-NCO GitHub repository, which comprises 10,000 instances for each problem variant (i.e., TSP, CVRP, PCTSP, and OP). Following

Table 15: Performance evaluation for different problems under different evaluation scenarios.

Method	TSP100 Gap	TSP100 Time	CVRP100 Gap	CVRP100 Time	OP100 Gap	OP100 Time	PCTSP100 Gap	PCTSP100 Time
The evaluation scenario of URS, the number of instances is 1000. Multi-start rollout and instance augmentation×8 are both applied.								
Oracle Solver	0.00%	6m	0.00%	9.1m	0.00%	1.5m	0.00%	1.2h
Sym-NCO	0.14%	5s	**1.46%**	6s	0.68%	15s	0.14%	16s
URS-STL	**0.08%**	6s	1.63%	6s	**0.11%**	4s	**-0.09%**	5s
URS	0.57%	6s	1.81%	6s	0.45%	4s	1.06%	5s
In the evaluation scenario of Sym-NCO, the number of instances is 10000. Only multi-start rollout is applied.								
Oracle Solver	0.00%	21m	0.00%	13h	0.00%	15m	0.00%	12h
Sym-NCO	0.39%	8s	**1.46%**	10s	0.45%	2.6m	-0.02%	2.7m
URS-STL	**0.30%**	7s	1.80%	8s	**-0.02%**	10.6s	**-0.06%**	11.7s
URS	1.24%	7s	2.03%	8s	0.50%	10.6s	1.30%	11.7s

Table 16: Performance comparison with POMO and Sym-NCO in real-world instances in TSPLIB with $50 < N < 250$.

Instance	Opt.	POMO aug×20 Obj.	POMO aug×20 Gap	Sym-NCO aug×20 Obj.	Sym-NCO aug×20 Gap	URS-STL aug×8 Obj.	URS-STL aug×8 Gap	URS aug×8 Obj.	URS aug×8 Gap
eil51	426	429	0.82%	432	1.39%	430	0.94%	427	**0.23%**
berlin52	7,542	7,545	0.04%	7,544	0.03%	7,542	**0.00%**	7,543	0.01%
st70	675	677	0.31%	677	0.31%	675	**0.00%**	677	0.30%
pr76	108,159	108,681	0.48%	108,388	0.21%	108,159	**0.00%**	109,089	0.86%
eil76	538	544	1.18%	544	1.18%	538	**0.00%**	543	0.93%
rat99	1,211	1,270	4.90%	1,261	4.17%	1,212	**0.08%**	1,252	3.39%
rd100	7,910	7,912	0.03%	7,911	0.02%	7,910	**0.00%**	7,927	0.21%
KroA100	21,282	21,486	0.96%	21,397	0.54%	21,282	**0.11%**	21,572	1.36%
KroB100	22,141	22,285	0.65%	22,378	1.07%	22,146	**0.02%**	22,667	2.38%
KroC100	20,749	20,755	0.03%	20,930	0.87%	20,749	**0.00%**	20,772	0.11%
KroD100	21,294	21,488	0.91%	21,696	1.89%	21,294	**0.00%**	21,704	1.93%
KroE100	22,068	22,196	0.58%	22,313	1.11%	22,121	**0.24%**	22,192	0.56%
eil101	629	641	1.84%	641	1.84%	630	**0.16%**	640	1.75%
lin105	14,379	14,690	2.16%	14,358	0.54%	14,379	**0.00%**	14,754	2.61%
pr124	59,030	59,353	0.55%	59,202	0.29%	59,030	**0.00%**	59,942	1.54%
bier127	118,282	125,331	5.96%	122,664	3.70%	119,975	**1.43%**	122,941	3.94%
ch130	6,110	6,112	**0.03%**	6,118	0.14%	6,116	0.10%	6,184	1.21%
pr136	96,772	97,481	0.73%	97,579	0.83%	97,447	**0.70%**	98,197	1.47%
pr144	58,537	59,197	1.13%	58,930	0.67%	58,673	**0.23%**	58,981	0.76%
kroA150	26,524	26,833	1.16%	26,865	1.28%	26,591	**0.25%**	27,368	3.18%
kroB150	26,130	26,596	1.78%	26,648	1.98%	26,237	**0.41%**	26,900	2.95%
pr152	73,682	74,372	0.94%	75,292	2.18%	74,056	**0.51%**	75,453	2.40%
u159	42,080	42,567	1.16%	42,602	1.24%	42,427	**0.82%**	42,775	1.65%
rat195	2,323	2,546	9.58%	2,502	7.70%	2,379	**2.41%**	2,420	4.18%
kroA200	29,368	29,937	1.94%	29,816	1.53%	29,677	**1.05%**	30,419	3.58%
ts225	126,643	131,811	4.08%	127,742	**0.87%**	128,522	1.48%	129,233	2.05%
tsp225	3,919	4,149	5.87%	4,126	5.27%	4,000	**2.15%**	4,058	3.63%
pr226	80,369	82,428	2.56%	82,337	2.45%	81,707	**1.66%**	82,049	2.09%
Avg.Gap		1.87%		1.62%		**0.52%**		1.83%	

Sym-NCO, we employ an N-start rollout without applying instance augmentation for TSP and CVRP. For PCTSP and OP, the AM-based Sym-NCO employs a 200-sample approach. To ensure a fair comparison, we apply an additional coordinate transformation $(1 - x, 1 - y)$ to URS to match this sampling budget. Like Sym-NCO, we also tested the solvers on small-scale TSPLib data ($50 < \text{N} < 250$).

The comparison results under Sym-NCO's evaluation settings are presented in Table 15 and Table 16. According to the results, URS delivers impressive performance that is comparable to or even surpasses Sym-NCO, under Sym-NCO's own evaluation scenarios. This confirms that the performance of URS is robust and not dependent on a specific evaluation setting. Unlike Sym-NCO, which is a specialized solver trained individually for each problem using distinct models (POMO for TSP and CVRP; AM for PCTSP and OP) and specific hyperparameter tuning, URS achieves competitive results across a wide range of problems with a single set of parameters, highlighting its strong generalization capability.

J.3 Results on Benchmark Dataset

Our test results on Benchmark datasets are presented in Table 17 and Table 18. All models are trained on instances of size $N = 100$.

In Set-X dataset, some results for comparative models are sourced from MVMoE (Zhou et al., 2024b) and RouteFinder (Berto et al., 2024). As shown in Table 17, URS maintains its position as the best overall performance across instances of varying scales. Notably, RL-based URS surpasses the SL-based representative specialized model LEHD (8.678% vs. 12.836%), underscoring its practical applicability in real-world scenarios.

For CVRPLib XXL benchmark. The results in Table 18 clearly demonstrate that URS can significantly outperform existing multi-task neural routing solvers, especially on large-scale instances. Notably, URS also greatly surpasses many representative specialized models (e.g., LEHD, BQ, and ELG). These results further underscore the practical applicability of URS in real-world scenarios.

Table 17: Results on large-scale CVRPLIB instances (Set-X) (Uchoa et al., 2017) ($500 \leq N \leq 1000$). All models are trained on instances of size $N = 100$.

Set-X		POMO		LEHD		MTPOMO		MVMoE/4E		MVMoE/4E-L		RF-MVMoE		RF-TE		URS	
Instance	Opt.	Obj.	Gap	Obj.	Gap	Obj.	Gap	Obj.	Gap	Obj.	Gap	Obj.	Gap	Obj.	Gap	Obj.	Gap
X-n502-k39	69226	75617	9.232%	71438	3.195%	77284	11.640%	73533	6.222%	74429	7.516%	76338	10.274%	71791	3.705%	**71281**	**2.969%**
X-n513-k21	24201	30518	26.102%	**25624**	**5.880%**	28510	17.805%	32102	32.647%	31231	29.048%	32639	34.866%	28465	17.619%	26166	8.119%
X-n524-k153	154593	201877	30.586%	280556	81.480%	192249	24.358%	186540	20.665%	182392	17.982%	**170999**	**10.612%**	174381	12.800%	175250	13.362%
X-n536-k96	94846	106073	11.837%	103785	9.425%	106514	12.302%	109581	15.536%	108543	14.441%	105847	11.599%	103272	8.884%	**102969**	**8.564%**
X-n548-k50	86700	103093	18.908%	90644	4.549%	94562	9.068%	95894	10.604%	95917	10.631%	104289	20.287%	100956	16.443%	**89768**	**3.539%**
X-n561-k42	42717	49370	15.575%	**44728**	**4.708%**	47846	12.007%	56008	31.114%	51810	21.287%	53383	24.969%	49454	15.771%	45964	7.601%
X-n573-k30	50673	83545	64.871%	**53482**	**5.543%**	60913	20.208%	59473	17.366%	57042	12.569%	61524	21.414%	55952	10.418%	54361	7.278%
X-n586-k159	190316	229887	20.792%	232867	22.358%	208893	9.761%	215668	13.321%	214577	12.748%	212151	11.473%	205575	8.018%	**202645**	**6.478%**
X-n599-k92	108451	150572	38.839%	115377	6.386%	120333	10.956%	128949	18.901%	125279	15.517%	126578	16.714%	116560	7.477%	**114423**	**5.507%**
X-n613-k62	59535	68451	14.976%	**62484**	**4.953%**	67984	14.192%	82586	38.718%	74945	25.884%	73456	23.383%	67267	12.987%	65901	10.693%
X-n627-k43	62164	84434	35.825%	67568	8.693%	73060	17.528%	70987	14.193%	70905	14.061%	70414	13.271%	67572	8.700%	**66499**	**6.973%**
X-n641-k35	63682	75573	18.672%	68249	7.172%	72643	14.071%	75329	18.289%	72655	14.090%	71975	13.023%	70831	11.226%	**67005**	**5.218%**
X-n655-k131	106780	127211	19.134%	117532	10.069%	116988	9.560%	117678	10.206%	118475	10.952%	119057	11.497%	112202	5.078%	**110237**	**3.237%**
X-n670-k130	146332	208079	42.197%	220927	50.977%	190118	29.922%	197695	35.100%	183447	25.364%	**168226**	**14.962%**	168999	15.490%	184010	25.748%
X-n685-k75	68205	79482	16.534%	**72946**	**6.951%**	80892	18.601%	97388	42.787%	89441	31.136%	82269	20.620%	77847	14.137%	75942	11.344%
X-n701-k44	81923	97843	19.433%	86327	5.376%	92075	12.392%	98469	20.197%	94924	15.870%	90189	10.090%	89932	9.776%	**86038**	**5.023%**
X-n716-k35	43373	51381	18.463%	46502	7.214%	52709	21.525%	56773	30.895%	52305	20.593%	52250	20.467%	49669	14.516%	**46496**	**7.200%**
X-n733-k159	136187	159098	16.823%	149115	9.493%	161961	18.925%	178322	30.939%	167477	22.976%	156387	14.833%	148463	9.014%	**147743**	**8.485%**
X-n749-k98	77269	87786	13.611%	**83439**	**7.985%**	90582	17.229%	100438	29.985%	94497	22.296%	92147	19.255%	85171	10.227%	83759	8.399%
X-n766-k71	114417	135464	18.395%	131487	14.919%	144041	25.891%	152352	33.155%	136255	19.086%	130505	14.061%	**129935**	**13.563%**	139371	21.810%
X-n783-k48	72386	90289	24.733%	**76766**	**6.051%**	83169	14.897%	100383	38.677%	92960	28.423%	96336	33.087%	83185	14.919%	77437	6.978%
X-n801-k40	73305	124278	69.536%	77546	5.785%	85077	16.059%	91560	24.903%	87662	19.585%	87118	18.843%	86164	17.542%	**77369**	**5.544%**
X-n819-k171	158121	193451	22.344%	178558	12.925%	177157	12.039%	183599	16.113%	185832	17.525%	179596	13.581%	174441	10.321%	**171024**	**8.160%**
X-n837-k142	193737	237884	22.787%	207709	7.212%	214207	10.566%	229526	18.473%	221286	14.220%	230362	18.904%	208528	7.635%	**203457**	**5.017%**
X-n856-k95	88965	152528	71.447%	**92936**	**4.464%**	101774	14.398%	99129	11.425%	106816	20.065%	105801	18.924%	98291	10.483%	94547	6.274%
X-n876-k59	99299	119764	20.609%	**104183**	**4.918%**	116617	17.440%	119619	20.463%	114333	15.140%	114016	14.821%	107416	8.174%	105417	6.161%
X-n895-k37	53860	70245	30.421%	**58028**	**7.739%**	65587	21.773%	79018	46.710%	64310	19.402%	69099	28.294%	64871	20.444%	58137	7.941%
X-n916-k207	329179	399372	21.324%	385208	17.021%	361719	9.885%	383681	16.557%	374016	13.621%	373600	13.494%	352998	7.236%	**346556**	**5.279%**
X-n936-k151	132715	237625	79.049%	196547	48.097%	186262	40.347%	220926	66.466%	190407	43.471%	**161343**	**21.571%**	163162	22.942%	172675	30.110%
X-n957-k87	85465	130850	53.104%	**90295**	**5.651%**	98198	14.898%	113882	33.250%	105629	23.593%	123633	44.659%	102689	20.153%	90485	5.874%
X-n979-k58	118976	147687	24.132%	127972	7.561%	138092	16.067%	146347	23.005%	139682	17.404%	131754	10.740%	129952	9.225%	**125353**	**5.360%**
X-n1001-k43	72355	100399	38.759%	**76689**	**5.990%**	87660	21.153%	114448	58.176%	94734	30.929%	88969	22.962%	85929	18.760%	77739	7.441%
Avg. Gap		29.658%		12.836%		16.796%		26.408%		19.607%		18.795%		12.303%		**8.678%**	

Table 18: Comparison on CVRPLib Set-XXL with scale $\in [3000, 7000]$. All models are trained on instances of size N = 100.

Method	Type	Leuven1 (N=3000)	Leuven2 (N=4000)	Antwerp1 (N=6000)	Antwerp2 (N=7000)	Total N $\in$ [3000,7000]
LEHD greedy	Specialized	16.60%	34.86%	14.66%	22.77%	22.22%
BQ greedy	Specialized	18.53%	30.70%	16.48%	27.67%	23.34%
POMO aug×8	Specialized	460.32%	202.17%	OOM	OOM	–
Sym-NCO aug×8	Specialized	196.82%	328.17%	OOM	OOM	–
ELG aug×8	Specialized	12.12%	21.52%	OOM	OOM	–
MTPOMO aug×8	General	67.72%	87.31%	OOM	OOM	–
MVMoE/4E aug×8	General	299.10%	170.10%	OOM	OOM	–
MVMoE/4E-L aug×8	General	182.28%	127.07%	OOM	OOM	–
RF-MVMoE aug×8	General	57.30%	160.27%	OOM	OOM	–
RF-TF aug×8	General	26.90%	45.56%	OOM	OOM	–
CaDA aug×8	General	1035.51%	OOM	OOM	OOM	–
ReLD-MTL aug×8	General	17.00%	30.59%	OOM	OOM	–
GOAL greedy	General	OOM	OOM	OOM	OOM	–
URS aug×8	General	**11.57%**	**17.80%**	**9.23%**	**14.95%**	**13.39%**

J.4 Scalability to Larger-scale Realistic Problems

Due to the limited benchmark datasets currently available for VRP variants, we have conducted further experiments on large-scale synthetic problem instances to validate the large-scale cross-problem generalization ability of URS. We generate a new large-scale (1K-5K nodes) synthetic dataset for a diverse set of problems (CVRPTW, CVRPB, and OCVRPTW). Each dataset contains 16 instances. For all instances, we adhere to the capacity constraints specified in TAM (Hou et al., 2022). To ensure a fair comparison, HGS-PyVRP is executed with multi-core (16) parallelism enabled, which allows it to process all instances of a specific size concurrently. According to the results, our proposed URS consistently achieves the best solution quality, complemented by remarkably fast inference times, across various problem instances among all comparable neural solvers. The advantages of URS over existing multi-task neural solvers are significant. Remarkably, URS already outperforms the strong HGS-PyVRP with a carefully manual design on large-scale CVRPB instances. These extensive new results demonstrate URS's strong scalability and generalization ability to large-scale and realistic problems.

Table 19: Generalization performance on large-scale instances of different VRP variants. All models are trained on instances of size N = 100 and employ instance augmentation × 8. Each dataset includes 16 instances. Note that "Time" is the total running time, and HGS-PyVRP is executed with multi-core (16) parallelism enabled.

Problem	Method	N = 1000 Obj.(Gap)	Time	N = 2000 Obj.(Gap)	Time	N = 3000 Obj.(Gap)	Time	N = 4000 Obj.(Gap)	Time	N = 5000 Obj.(Gap)	Time
CVRPTW	HGS-PyVRP	159.35(0.00%)	20m	337.15(0.00%)	40m	516.97(0.00%)	1h	618.58(0.00%)	2.7h	787.25(0.00%)	3.3h
	MTPOMO	219.22(37.57%)	1.7m	488.40(44.86%)	14.6m	773.00(49.53%)	49.5m	975.61(57.72%)	1.9h	OOM	
	MVMoE	233.53(46.55%)	1.7m	624.73(85.30%)	14.6m	1094.25(111.67%)	51.9m	1486.34(140.28%)	2h	OOM	
	ReLD-MTL	183.31(15.036%)	1.6m	396.28(17.54%)	13.4m	613.58(18.69%)	45.7m	748.65(21.03%)	1.8h	OOM	
	URS-MTL	**172.58(8.30%)**	**1.3m**	**365.27(8.34%)**	**11.1m**	**559.03(8.14%)**	**30.1m**	**673.63(8.90%)**	**1.2h**	**853.79(8.45%)**	**2.3h**
CVRPB	HGS-PyVRP	36.52(0.00%)	20m	51.80(0.00%)	40m	75.12(0.00%)	1h	93.52(0.00%)	2.7h	112.21(0.00%)	3.3h
	MTPOMO	45.92(25.77%)	1.1m	83.50(61.20%)	8.8m	136.52(81.73%)	31.4m	197.99(111.70%)	1.2h	OOM	
	MVMoE	98.60(170.03%)	1m	250.47(383.57%)	8.1m	332.93(343.19%)	28.9m	423.19(352.49%)	1.1h	OOM	
	ReLD-MTL	38.52(5.48%)	1m	59.21(14.30%)	8m	88.36(17.62%)	28.3m	114.88(22.83%)	1.1h	OOM	
	URS-MTL	**34.86(-4.54%)**	**40s**	**50.39(-2.72%)**	**5.1m**	**72.01(-4.15%)**	**17.3m**	**91.74(-1.91%)**	**41.2m**	**111.93(-0.24%)**	**1.3h**
OCVRPTW	HGS-PyVRP	90.91(0.00%)	20m	164.00(0.00%)	40m	224.16(0.00%)	1h	299.45(0.00%)	2.7h	367.86(0.00%)	3.3h
	MTPOMO	147.14(61.85%)	1.6m	297.53(81.43%)	12.8m	437.73(95.28%)	44.3m	601.63(100.91%)	1.7h	OOM	
	MVMoE	147.35(62.09%)	1.6m	389.60(137.57%)	12.9m	634.11(182.88%)	44.7m	899.18(200.28%)	1.7h	OOM	
	ReLD-MTL	110.00(21.01%)	1.5m	208.60(27.20%)	12.3m	292.70(30.57%)	42m	394.42(31.72%)	1.6h	OOM	
	URS-MTL	**98.76(8.63%)**	**1m**	**178.07(8.58%)**	**7.6m**	**243.88(8.80%)**	**25.4m**	**325.64(8.74%)**	**1h**	**398.72(8.39%)**	**1.9h**

K Ablation Study

In this section, we conduct a detailed ablation study and analysis to demonstrate the effectiveness and robustness of URS. Please note that, unless stated otherwise, the results presented in the ablation study reflect the best result from multiple trajectories, and we employ instance augmentation to improve performance in the ablation study. We adopt the widely used 100-node setting as our primary evaluation scenario for URS.

K.1 Effects of Node-type Indicator

Table 20: The ablation study of the node-type indicator on trained VRPs

Method	ATSP	TSP	OP	PCTSP	PDTSP	ACVRP	CVRP	CVRPTW	CVRPB	OCVRP	OCVRPTW	Avg.gap
w/o $\boldsymbol{\xi}_i$	**2.14%**	**0.48%**	0.45%	1.06%	9.28%	**2.84%**	3.66%	6.61%	1.57%	7.87%	5.66%	3.78%
w/ $\boldsymbol{\xi}_i$	2.26%	0.57%	**0.45%**	**1.06%**	**4.98%**	3.06%	**1.81%**	**6.13%**	**1.46%**	**3.24%**	**5.07%**	**2.74%**

To evaluate the effectiveness of node-type indicator $\boldsymbol{\xi}$, we conduct an ablation study about including and excluding $\boldsymbol{\xi}$. Table 20 shows that adding the node-type indicator reduces the average optimality gap from 3.78% to 2.74%, with large gains on the routing problem with relatively rich instance node roles, such as PDTSP, where the coexistence of a depot and paired pickup–delivery nodes (with inherent precedence coupling) allows the explicit node-role encoding to further boost performance. Meanwhile, URS maintains a competitive performance in addressing the problem of single-node roles.

K.2 Effects of Problem State

Table 21: Performance impact of removing the problem state feature C_t

Method	ATSP	TSP	OP	PCTSP	PDTSP	ACVRP	CVRP	CVRPTW	CVRPB	OCVRP	OCVRPTW	Avg.gap
w/o C_t	**2.09%**	**0.45%**	0.60%	1.20%	**4.59%**	4.03%	2.70%	**5.71%**	2.64%	4.02%	**4.62%**	2.97%
w/ C_t	2.26%	0.57%	**0.45%**	**1.06%**	4.98%	**3.06%**	**1.81%**	6.13%	**1.46%**	**3.24%**	5.07%	**2.74%**

As described in Appendix E.3, the majority of VRP variants are already solved without supplying an additional problem state C_t. To test whether the remaining use of C_t matters, we conduct an ablation in which we eliminate it entirely, enforcing $C_t \equiv 0$ for all problems. The results in Table 21 show that URS maintains its competitive performance even in the absence of C_t. This indicates that explicit constraint-state features are not essential for the effectiveness of URS. Interestingly, on (O)CVRPTW instances, the model without any explicit constraint features outperforms the version that supplies only capacity information. We guess that capacity and time windows information are equally important, so enforcing only capacity creates a bias toward load considerations.

K.3 Effects of Mixed Bias Module

Table 22: Ablation of prior components in the Mixed Bias Module (MBM).

$\boldsymbol{D}$	$\boldsymbol{D}^{\mathbf{T}}$	$\boldsymbol{R}$	ATSP	TSP	OP	PCTSP	PDTSP	ACVRP	CVRP	CVRPTW	CVRPB	OCVRP	OCVRPTW	Avg.gap
✓	×	×	16.64%	**0.44%**	**0.25%**	**0.67%**	7.33%	16.62%	2.42%	6.44%	3.96%	9.44%	5.47%	6.33%
✓	✓	×	**2.09%**	0.45%	0.48%	0.82%	7.66%	9.11%	2.52%	6.89%	2.68%	5.70%	6.36%	4.07%
✓	×	✓	16.60%	0.46%	0.49%	0.94%	**4.49%**	26.22%	4.16%	6.57%	3.07%	12.23%	5.53%	7.34%
✓	✓	✓	2.26%	0.57%	0.45%	1.06%	4.98%	**3.06%**	**1.81%**	**6.13%**	**1.46%**	**3.24%**	**5.07%**	**2.74%**

To further assess the effectiveness of MBM, we conduct an ablation study that incorporates different combinations of problem-specific priors into the MBM. Owing to its flexibility, the MBM permits imposing multiple priors on the same shared attention layer. The results in Appendix K.3 underscore the complementary roles of the three prior components: (1) The transposed distance matrix $\boldsymbol{D}^{\mathbf{T}}$ captures directional asymmetry absent from the raw distance matrix, and its inclusion markedly stabilizes optimization on asymmetric variants; (2) Removing the pickup–delivery relation matrix $\boldsymbol{R}$ degrades performance on PDTSPs, confirming that explicit relational coupling is indispensable

for these instances; (3) When all priors are fused, MBM can simultaneously learn the geometric and relational biases inherent in various problems, yielding the best overall performance.

K.4 Effects of Different Decoder Architectures

Table 23: Effect of different decoder architectures on URS cross-problem performance

Decoder	ATSP	TSP	OP	PCTSP	PDTSP	ACVRP	CVRP	CVRPTW	CVRPB	OCVRP	OCVRPTW	Avg.gap
URS-POMO	4.83%	0.74%	0.72%	1.29%	5.45%	5.09%	1.99%	6.42%	1.83%	3.62%	5.31%	3.39%
URS-ReLD	6.48%	0.90%	0.86%	1.51%	5.81%	6.51%	2.33%	6.56%	2.33%	3.62%	5.64%	3.87%
URS	**2.26%**	**0.57%**	**0.45%**	**1.06%**	**4.98%**	**3.06%**	**1.81%**	**6.13%**	**1.46%**	**3.24%**	**5.07%**	**2.74%**

We adopt an AM (Kool et al., 2019) as our basic encoder-decoder model. Multiple decoder refinements have been proposed around AM (Kwon et al., 2020; Huang et al., 2025; Zhou et al., 2024a). To assess how decoder structure impacts multi-task performance, we additionally train two URS variants whose decoders follow POMO and ReLD, denoted URS-POMO and URS-ReLD. For stronger and fairer baselines, we apply Distance-aware Attention Reshaping (DAR) (Wang et al., 2025b) to both, and all decoder parameters are generated by a hypernetwork conditioned on the problem representation $\boldsymbol{\lambda}$ (see Appendix E.2). As shown in Table 23, URS-POMO and URS-ReLD still exhibit strong cross-problem robustness, while replacing the decoder with ICAM (Zhou et al., 2024a) yields a further overall improvement.

K.5 Effects of Different Components on Zero-shot Generalization

Table 24: Ablation of different components in the model architecture, which includes MBM, WEIGHT(λ), and BIAS(λ). The symbol (*) indicates the seen problems in training.

MBM	WEIGHT(λ)	BIAS(λ)	ATSP (*)	TSP (*)	OP (*)	PCTSP (*)	PDTSP (*)	ACVRP (*)
×	✓	✓	16.64%	**0.44%**	**0.25%**	**0.67%**	7.33%	16.62%
✓	×	✓	3.24%	1.10%	1.04%	1.42%	6.38%	4.07%
✓	✓	×	3.83%	1.16%	1.09%	1.52%	6.65%	4.27%
✓	×	×	4.79%	1.58%	1.39%	1.92%	7.05%	5.39%
✓	✓	✓	**2.26%**	0.57%	0.45%	1.06%	**4.98%**	**3.06%**

MBM	WEIGHT(λ)	BIAS(λ)	CVRP (*)	CVRPTW (*)	CVRPB (*)	OCVRP (*)	OCVRPTW (*)	CVRPL
×	✓	✓	2.42%	6.44%	3.96%	9.44%	5.47%	0.98%
✓	×	✓	4.23%	6.52%	3.00%	3.99%	5.41%	2.92%
✓	✓	×	9.94%	6.18%	5.00%	4.61%	5.21%	4.79%
✓	×	×	2.90%	6.60%	3.12%	4.47%	5.76%	1.46%
✓	✓	✓	**1.81%**	**6.13%**	**1.46%**	**3.24%**	**5.07%**	**0.43%**

MBM	WEIGHT(λ)	BIAS(λ)	OCVRPB	CVRPBL	CVRPLTW	OCVRPBTW	CVRPBLTW	OCVRPL
×	✓	✓	15.95%	4.18%	2.89%	18.78%	10.93%	9.51%
✓	×	✓	9.54%	5.30%	2.73%	14.37%	9.80%	4.64%
✓	✓	×	9.58%	3.25%	3.07%	14.16%	9.91%	3.88%
✓	×	×	9.92%	3.34%	3.08%	14.02%	9.92%	4.52%
✓	✓	✓	**9.35%**	**1.65%**	**2.67%**	**13.77%**	**9.18%**	**3.22%**

MBM	WEIGHT(λ)	BIAS(λ)	CVRPBTW	OCVRPBL	OCVRPLTW	OCVRPBLTW	Avg.gap	Best Sol.
×	✓	✓	10.74%	16.14%	5.57%	18.80%	8.37%	3/22
✓	×	✓	9.67%	10.67%	5.23%	14.49%	5.90%	0/22
✓	✓	×	9.63%	10.42%	5.51%	13.99%	6.26%	0/22
✓	×	×	9.79%	10.02%	5.81%	13.98%	5.95%	0/22
✓	✓	✓	**8.94%**	**9.47%**	**5.12%**	**13.72%**	**3.88%**	**19/22**

To empirically evaluate the necessity of these components, we have conducted tests on the 11 seen problems as well as 11 additional unseen CVRP variants widely investigated in current multi-task research (e.g., MVMoE (Zhou et al., 2024b)). The results are presented in Table 24. We can observe that removing MBM leads to a significant performance drop on problems with complex geometric properties, such as ATSP, ACVRP, and PDTSP, which confirms MBM is critical for perceiving specific geometric biases. In addition, removing WEIGHT(λ) or BIAS(λ) also results in performance degradation across most tasks. In terms of overall performance, URS significantly outperforms any model where a single module is removed. The full URS model achieves the lowest average gap and

provides the best solution on the majority of tasks (19/22). This demonstrates that the synergy of these components is essential for robust cross-problem generalization.

L LICENSES FOR USED RESOURCES

Table 25: List of licenses for the codes and datasets we used in this work.

Resource	Type	Link	License
HGS-PyVRP (Wouda et al., 2024)	Code	https://github.com/PyVRP/PyVRP	MIT License
LKH3 (Helsgaun, 2017)	Code	http://webhotel4.ruc.dk/~keld/research/LKH-3/	Available for academic research use
OR-Tools (Perron & Furnon, 2023)	Code	https://github.com/google/or-tools	Apache-2.0 License
POMO (Kwon et al., 2020)	Code	https://github.com/yd-kwon/POMO/tree/master/NEW_py_ver	MIT License
Sym-NCO (Kim et al., 2022)	Code	https://github.com/alstn12088/Sym-NCO	Available for any non-commercial use
LEHD (Luo et al., 2023)	Code	https://github.com/CIAM-Group/NCO_code/tree/main/single_objective/LEHD	Available for any non-commercial use
BQ (Drakulic et al., 2023)	Code	https://github.com/naver/bq-nco	CC BY-NC-SA 4.0 license
ICAM (Zhou et al., 2024a)	Code	https://github.com/CIAM-Group/ICAM	MIT License
MatNet (Kwon et al., 2021)	Code	https://github.com/yd-kwon/MatNet/tree/main	MIT License
Heter-AM (Li et al., 2021)	Code	https://github.com/jingwenli0312/Heterogeneous-Attentions-PDP-DRL	MIT License
MTPOMO (Liu et al., 2024a)	Code	https://github.com/FeiLiu36/MTNCO	MIT License
MVMoE (Zhou et al., 2024b)	Code	https://github.com/RoyalSkye/Routing-MVMoE	MIT License
RouteFinder (Berto et al., 2024)	Code	https://github.com/ai4co/routefinder	MIT License
CaDA (Li et al., 2025a)	Code	https://github.com/CIAM-Group/CaDA	MIT License
ReLD (Huang et al., 2025)	Code	https://github.com/ziweileonhuang/reld-nco	MIT License
GOAL (Drakulic et al., 2025)	Code	https://github.com/naver/goal-co	Available for any non-commercial use
CVRPLIB Set-X (Uchoa et al., 2017)	Dataset	http://vrp.galgos.inf.puc-rio.br/index.php/en/	Available for academic research use

We list the used existing codes and datasets in Table 25, and all of them are open-sourced resources for academic usage.

M LLM USAGE

During the preparation of this manuscript, we utilized a Large Language Model (LLM) as a writing assistance tool. The primary purpose of its use was to improve the linguistic quality of the paper. Specifically, the LLM is used to polish the writing for enhanced clarity and fluency and to identify and correct grammatical, spelling, and punctuation errors.

We confirm that all core research ideas, study design, data analysis, and conclusions are independently developed by the authors. The LLM does not contribute to the research ideation, methodology, or substantive academic content of the paper. Its function was strictly confined to language editing and proofreading to ensure the manuscript's professionalism and readability.